Surface-associated antigen induces B-cell permeabilization and lysosome exocytosis facilitating antigen uptake and presentation to T-cells

Fernando Y. Maeda[1#], Jurriaan J. H. van Haaren[1#], David B. Langley[2], Daniel Christ[2,3], Norma W. Andrews[1]* and Wenxia Song[1]*

[1]Department of Cell Biology and Molecular Genetics, University of Maryland, College Park, MD 20742, USA.

[2]Immunology Division, Garvan Institute of Medical Research, Darlinghurst, NSW 2010, Australia

[3]St Vincent's Clinical School, University of New South Wales, Darlinghurst, NSW 2010, Australia

[#]These authors contributed equally to this study.

*Co-corresponding authors:

Wenxia Song: wenxsong@umd.edu

Norma Andrews: andrewsn@umd.edu

Abstract

B-cell receptor (BCR)-mediated antigen internalization and presentation are essential for humoral memory immune responses. Antigen encountered by B-cells is often tightly associated with the surface of pathogens and/or antigen-presenting cells. Internalization of such antigens requires myosin-mediated traction forces and extracellular release of lysosomal enzymes, but the mechanism triggering lysosomal exocytosis is unknown. Here we show that BCR-mediated recognition of antigen tethered to beads, to planar lipid-bilayers or expressed on cell surfaces causes localized plasma membrane (PM) permeabilization, a process that requires BCR signaling and non-muscle myosin II activity. B-cell permeabilization triggers PM repair responses involving lysosomal exocytosis, and B-cells permeabilized by surface-associated antigen internalize more antigen than cells that remain intact. Higher affinity antigens cause more B-cell permeabilization and lysosomal exocytosis and are more efficiently presented to T-cells. Thus, PM permeabilization by surface-associated antigen triggers a lysosome-mediated B-cell resealing response, providing the extracellular hydrolases that facilitate antigen internalization and presentation.

Introduction

B-cells are responsible for generating antibody responses that neutralize pathogens and attract other immune cells. B-cell activation is initiated by the B-cell receptor (BCR), which surveys antigen through its membrane-anchored immunoglobulin (Reth 1994). Antigen-BCR interaction induces signaling cascades and antigen internalization, followed by intracellular processing and surface presentation to T-cells. Antigen presentation is essential for the activation of B-cells and their differentiation into high-affinity memory or antibody-secreting cells (Shlomchik and Weisel 2012). A property that is critical for maximizing humoral protection is the ability of clonal-specific BCRs to recognize antigens in their different physical, chemical, and biological forms.

Antigen encountered by B-cells *in vivo* is often tightly associated with the surface of pathogens, such as parasites, bacteria and viruses, and/or antigen-presenting cells, such as follicular dendritic cells (Gonzalez *et al.* 2011). Internalization, processing, and presentation of such surface-bound antigens are essential for specific B-cells to obtain T-cell help, which is critical for B-cell activation and differentiation. Follicular dendritic cells, which are uniquely present in germinal centers of secondary lymphoid organs, internalize antigens that drain into these organs and present them to B-cells (Suzuki *et al.* 2009; Cyster 2010). Competition between high and low-affinity B-cells to acquire antigen from follicular dendritic cells is a critical step in the selection of high-affinity cells that differentiate into memory B-cells and long-lived plasma cells.

B-cells, follicular B-cells in particular, are thought to have a limited ability to phagocytose large insoluble antigen particles (Vidard *et al.* 1996). However, B-cells are able to extract and endocytose antigen that is tightly associated with non-internalizable surfaces (Batista and

Neuberger 2000). Importantly, the efficiency of antigen presentation by B-cells appears to depend more strongly on the BCR-antigen binding affinity when the antigen is associated with non-internalizable surfaces, compared to antigen bound to internalizable particles (Batista and Neuberger 2000). Recent studies using antigen-coated beads, planar lipid bilayers, or plasma membrane (PM) sheets revealed two major mechanisms by which B-cells extract antigen from non-internalizable surfaces for endocytosis. Mechanical forces, generated by non-muscle myosin II (NMII) activation at sites of antigen-BCR interaction, can directly pull antigen from presenting surfaces for endocytosis. When mechanical forces alone are not sufficient, hydrolases released from lysosomes cleave surface-associated antigen to facilitate internalization (Yuseff *et al.* 2011; Natkanski *et al.* 2013; Spillane and Tolar 2017; J. Wang *et al.* 2018). Surface-associated antigen was previously shown to induce polarization of B-cell lysosomes towards antigen-binding sites (Yuseff *et al.* 2011), but the mechanism responsible for triggering lysosome exocytosis and release of hydrolytic enzymes was unknown.

When cells are permeabilized by physical tearing or pore-forming proteins, Ca^{2+} influx triggers rapid exocytosis of lysosomes as part of the process that repairs the PM and prevents cell death (Reddy *et al.* 2001; Andrews *et al.* 2014). Since its discovery several decades ago (Rodríguez *et al.* 1997), Ca^{2+}-dependent exocytosis of lysosomes has been observed in many cell types (Zhang *et al.* 2007; Naegeli *et al.* 2017; Villeneuve *et al.* 2018; Ibata *et al.* 2019). We previously reported that permeabilization of the PM of mouse splenic B-cells with the pore-forming toxin streptolysin O (SLO) triggers lysosomal exocytosis, releasing hydrolases extracellularly and exposing the luminal epitope of the lysosome-associated protein LIMP-2 on the cell surface. B-cells rapidly reseal these PM lesions in a process that requires lysosomal exocytosis (Miller *et al.*

2015). Surprisingly, in this study we found that interaction of the BCR with surface-associated antigen can permeabilize the B-cell PM, triggering a resealing mechanism that involves exocytosis of lysosomes. We investigated this process by determining if antigen-induced PM permeabilization depends on the BCR-antigen binding affinity, BCR signaling and NMII motor activity, and if it influences the ability of B-cells to internalize and present surface-associated antigens to T-cells.

Results

BCR interaction with surface-associated antigen induces B-cell PM permeabilization at antigen-binding sites

We initially utilized two experimental models previously used to study BCR-mediated internalization of surface-associated antigen: $F(ab')_2$-anti-mouse IgM+G (αM, which binds and activates mouse BCRs) immobilized on beads or tethered to planar lipid bilayers (PLB) by biotin-streptavidin interaction. Beads or PLB coated with transferrin (Tf) at similar surface density as αM were used as controls, as Tf does not activate the BCR and interacts with the Tf receptor with similar affinity as the *bona fide* antigen hen egg lysozyme (HEL) binds to the BCR of transgenic MD4 mouse B-cells (Batista and Neuberger 1998; Fuchs and Gessner 2002). Strikingly, live imaging revealed influx of the membrane-impermeable dye propidium iodide (PI) at sites of primary B-cell contact with αM-beads, indicating that PM permeabilization occurred at bead-binding locations (*Figure 1A, Figure 1-figure supplement 1 and Videos 1-3*). While similar percentages of B-cells bound αM- or Tf-beads (*Figure 1B)*, a significantly higher fraction of B-cells binding αM-beads became PI-positive (*Figure 1C*). Flow cytometry analysis confirmed the increased PI entry in B-cells binding αM-beads when compared to Tf-beads

(*Figure 1D-G and Figure 1-figure supplement 2*). Addition of soluble F(ab')$_2$-anti-mouse IgM+G (sαM, also capable of binding and activating the BCR) did not increase the frequency of PI entry in B-cells binding to Tf-beads (*Figure 1F*). The percentage of cells positive for cleaved caspase-3, an early apoptotic marker, was similar in B-cells interacting or not with αM- or Tf-beads and only increased significantly after treatment with staurosporine (*Figure 1-figure supplement 3*), suggesting that PM permeabilization is not associated with apoptosis. Similar observations were made using the PLB system that allows lateral movement of the tethered antigen (Dustin *et al.* 2007). Significantly more B-cells became PI-positive when contacting αM-PLB when compared to Tf-PLB (*Figure 1H-J*).

PM permeabilization in B-cells binding to αM-PLB was also observed using membrane-impermeable lipophilic FM probes. These fluorescent dyes have been used extensively to assess PM integrity, because they only label the outer PM leaflet of intact cells but rapidly stain intracellular membranes when entering the cytosol (Bansal *et al.* 2003; McNeil *et al.* 2003; Demonbreun *et al.* 2019). After >30 min of interaction with αM-PLB, we observed sudden, massive increases in FM1-43 staining of intracellular membranes, including the nuclear envelope (*Figure 1H and I, Figure 1-figure supplements 4, 5 and Video 4*). Consistent with the PI entry results (*Figure 1J)*, significantly more B-cells showed a sudden increase in intracellular FM staining when contacting αM-PLB compared to Tf-PLB (*Figure 1K*). This characteristic pattern of sudden FM influx with staining of the nuclear envelope was only observed in B-cells that eventually became PI-positive, not in cells that remained PI-negative during interaction with αM-PLB (*Figure 1- figure supplement 4*). Since FM lipophilic dyes can also be internalized through surface receptor endocytosis, we activated BCR endocytosis by cross-linking surface

BCRs using soluble F(ab')$_2$ goat-anti-mouse IgM+G antibodies followed by fluorescent F(ab')$_2$ anti-goat-IgG (Song *et al.* 1995; Hoogeboom and Tolar 2016). Under these conditions, which did not cause PM permeabilization, we observed FM1-43 uptake appearing as small peripheral puncta that colocalized with BCR cross-linking antibodies. Such endosome-associated FM1-43 staining pattern was markedly different from the sudden, massive FM influx observed shortly before PI entry in permeabilized cells (*Figure 1-figure supplement 6* and *Video 4*). Collectively, these data show that the sudden, massive influx of FM dyes during αM-PLB binding is caused by B-cell permeabilization, and not by a gradual endocytosis of the PM-associated tracer triggered by BCR engagement.

As an independent method to demonstrate antigen-induced permeabilization of B-cells, we took advantage of the ability of membrane-impermeable Ponceau 4R to quench cytosolic fluorophores upon entering cells (Tay *et al.* 2019). Instead of monitoring nuclear or intracellular membrane staining by membrane-impermeable fluorescent dyes, we determined the percentage of B-cells pre-loaded with carboxyfluorescein succinimidyl ester (CFSE) that lost their cytosolic fluorescence as a consequence of Ponceau 4R entry during PM permeabilization. To validate this method, we first permeabilized B-cells with the pore-forming toxin streptolysin O (SLO). In the presence of Ponceau 4R, the percentage of B-cells with reduced CFSE fluorescence increased significantly after exposure to SLO (*Figure 2A and B*), mimicking what we previously observed for PI entry in SLO-treated B-cells (Miller *et al.* 2015). Thus, quenching of cytoplasmic CFSE by the membrane-impermeable Ponceau 4R is a potent indicator of PM permeabilization. Using this method, we compared B-cells incubated with αM- or Tf-PLB by live imaging. A significantly higher fraction of CFSE-labeled B-cells showed fluorescence quenching when

interacting with αM-PLB, quantified as the percentage of cells that lost >70% of their initial CFSE fluorescence (*Figure 2C and D and Video 5*). The average time for detection of αM-PLB-induced B-cell permeabilization measured by this quenching method was similar to what was observed for FM entry, while the average time for intracellular detection of PI showed a ~8 min delay (*Figure 2E, Figure 1-figure supplements 4 and Video 4*). An analysis of the cumulative rate of influx of the three distinct tracers confirmed the small delay in PI detection (*Figure 2F*). Thus, FM influx and Ponceau 4R-mediated quenching are more sensitive methods for detecting the onset of B-cell PM permeabilization when compared to PI influx, which is only clearly visualized after intercalation into double-stranded DNA inside the nucleus. Based on consistent results obtained with three different methods, we conclude that BCR binding to αM-coated surfaces (but not to soluble αM) causes localized permeabilization of the B-cell PM.

We next determined whether HEL, a *bona fide* antigen recognized by the BCR from MD4 mice, also caused B-cell permeabilization when tethered to artificial surfaces or presented as an integral membrane protein (mHEL) on the surface of live cells (Batista *et al.* 2001). Flow cytometry analysis revealed that similar fractions of MD4 B-cells become PI-positive after binding beads coupled to αM or to HEL (*Figure 3A-C*). In contrast, WT B-cells binding to HEL-beads showed a low percentage of PI-positive cells, similar to what is observed with Tf-beads (*Figure 1F and Figure 3A-C*). Importantly, transmembrane mHEL-GFP expressed on the surface of live COS-7 cells co-clustered with the BCR at sites of interaction with MD4 B-cells, followed by PI influx. This dramatic clustering pattern followed by permeabilization was not observed in WT B-cells, whose BCR is incapable of specifically recognizing HEL (*Figure 3D* and *Videos 6 and 7*). A significantly higher percentage of MD4 B-cells showed PI influx after interaction with

COS-7 cells expressing mHEL-GFP, when compared to WT B-cells (*Figure 3E*). The percentage of PI-positive MD4 B-cells was also significantly higher after incubation with mHEL-expressing COS-7 cells than with mock-transfected cells (*Figure 3F*). Collectively these results show that BCR binding to surface-associated antigen can cause permeabilization of the B-cell PM.

Antigen-induced B-cell permeabilization requires high-affinity BCR-antigen binding, BCR signaling, and NMII motor activity

High-affinity binding of the BCR to antigen associated with non-internalizable surfaces induces high levels of BCR signaling, cytoskeleton reorganization, and antigen endocytosis (Batista and Neuberger 1998; Batista and Neuberger 2000; Fleire *et al.* 2006). To examine the impact of the BCR binding affinity on antigen-induced PM permeabilization, we incubated MD4 B-cells with beads coated with equal densities of HEL or the duck egg lysozyme isoform DEL-I. The MD4 BCR binds DEL-I with >100 fold lower affinity than it binds HEL (Langley *et al.* 2017). As expected, the percentage of B-cells binding multiple beads was reduced when the BCR-antigen affinity decreased (*Figure 4-figure supplement 1A*), but B-cells binding one single bead were detected for both HEL and DEL-I and also Tf (*Figure 4-figure supplement 1*). In these single bead-bound populations, DEL-I-beads caused significantly less PI entry than HEL-beads (*Figure 4A*). Inhibition of signaling with the Src kinase inhibitor PP2 (Cheng *et al.* 2001) (iSrc) or the Bruton's Tyrosine Kinase inhibitor AVL-292 (Aalipour and Advani 2013) (iBTK) (*Figure 4B and C*) also reduced PI entry in cells binding HEL-beads (*Figure 4D*). After contact with αM-PLB or αM-beads but not Tf-PLB or Tf-beads, surface BCRs became polarized towards PLB- or bead-binding sites within ~10 min, a period markedly shorter than what is required for detection of PM permeabilization through FM influx (*Figure 4E-H, Figure 4-figure supplement 2, and*

196 *Video 8*). Importantly, the activated form of the actin motor protein NMII, detected through its
197 phosphorylated light chain (pMLC), accumulated along with the BCR at αM-bead-binding sites
198 (*Figure 4G, Figure 4-figure supplement 3 and Video 9*). The fluorescence intensity ratios (FIR)
199 of surface BCRs and pMLC were significantly higher in B-cells binding αM-beads than in cells
200 binding Tf-beads (*Figure* 4*H and I*). Notably, inhibition of NMII motor activity with blebbistatin
201 (Bleb) markedly reduced the number of B-cells that became PI-positive during interaction with
202 αM-beads, without affecting the cells' ability to bind the beads (*Figure 4J and K*). Live imaging
203 detected PI entry following a "tug-of-war' between two B-cells simultaneously engaging an αM-
204 bead (*Video 3 and Figure 1-figure supplement 1C*), further supporting a role for NMII-mediated
205 traction forces in antigen-induced PM permeabilization. Thus, our results indicate that PM
206 permeabilization caused by surface-associated antigen requires strong BCR-antigen interaction
207 and the subsequent activation of signaling and NMII motor activity.
208
209 **Antigen-induced B-cell permeabilization triggers lysosomal exocytosis as a PM repair**
210 **response**
211 Permeabilization with the pore-forming toxin SLO triggers exocytosis of lysosomes in mouse
212 primary B-cells (Miller *et al.* 2015), a response to Ca^{2+} influx that is observed in several cell
213 types and is required for the resealing PM wounds (Reddy *et al.* 2001). To determine if
214 permeabilization by surface-associated αM or HEL triggered exocytosis of lysosomes in B-cells,
215 we first examined whether luminal epitopes of the lysosomal membrane protein LIMP-2 were
216 exposed on the cell surface. Flow cytometry detected surface LIMP-2 in a higher percentage of
217 B-cells binding αM-beads than in B-cells binding Tf-beads (*Figure 5A and B*). Notably, surface
218 exposure of LIMP-2 was lower in MD4 B-cells binding DEL-I-beads compared to HEL-beads

(*Figure 5C*). These results reveal a close correlation between the extent of PM permeabilization (*Figure 4A*) and lysosomal exocytosis induced by surface-associated αM, HEL or DEL-I (*Figure 5B-C*). Surface LIMP-2 was predominantly detected at sites of αM-bead binding (*Figure 5D and Figure 5-figure supplement 1*) and this polarized pattern, measured by FIR, increased after ~30 min of interaction with αM- but not Tf-beads (*Figure 5E*). Notably, this timeframe was similar to the average period required for PM permeabilization (*Figure 2E*). Next, we performed live total internal reflection fluorescence (TIRF) microscopy of B-cells preloaded with the luminal lysosomal probe SiR-Lyso (a membrane-permeable fluorescent peptide that binds to the lysosomal enzyme cathepsin D) while contacting αM-PLB. Exocytosis events were identified by rises in the fluorescence intensity of SiR-Lyso puncta (reflecting lysosome entry into the TIRF evanescent field adjacent to the PM) followed by sharp decreases within ~2 s (reflecting dye dispersion upon fusion of lysosomes with the PM) (*Figure 5F and G, Figure 5-figure supplement 2 and Video 10*). Exocytosis events were observed in the majority of individual PI-positive cells interacting with αM-PLB (*Figure 5H*) and occurred predominantly ~30-45 min after αM-PLB contact (*Figure 5H and I*), a timing similar to PM permeabilization and LIMP-2 exposure. Lysosomal exocytosis events were significantly more frequent in permeabilized B-cells when compared to B-cells that remained intact (*Figure 5J*). These results show that permeabilization of B-cells by surface-associated antigen triggers exocytosis of lysosomes.

We next determined if B-cells were capable of resealing their PM, by using an assay involving sequential exposure to two different membrane-impermeable fluorescent dyes (Reddy *et al.* 2001). Resealed cells were quantified by flow cytometry as the percentage of permeabilized cells binding αM-beads (stained intracellularly with FM4-64 kept throughout the assay) that excluded

the membrane-impermeable dye SYTOX Blue (added only during the last 10 min of the assay) (*Figure 6A*). Under these conditions, ~50% of B-cells permeabilized by surface-associated antigen resealed their PM within the assay period (*Figure 6B*). Inhibition of lysosomal exocytosis with bromoenol lactone (BEL) (Fensome-Green *et al.* 2007; Tam *et al.* 2010) significantly reduced the percentage of resealed cells (*Figure 6A and B*). We found no evidence that the reduction in resealed cells after BEL treatment was due to toxicity of this inhibitor. B-cell populations with low forward-scatter versus side-scatter values typical of dead cells did not increase after BEL treatment (*Figure 6-figure supplement 1*). Exposure to BEL also did not increase the small fraction (<7%) of Tf-bead-binding B-cells that was permeable to SYTOX Blue (*Figure 6-figure supplement 1*). These data suggest that lysosomal exocytosis is required for the resealing of B-cells permeabilized by binding to surface-associated antigen. To confirm that individual antigen-permeabilized B-cells resealed, we used live imaging to visualize cells incubated with αM-PLB in the presence of SYTOX Green. PI was then added for the last 10 min of the 4 h incubation. Time-lapse images showed that B-cells that became permeable to SYTOX Green during interaction with αM-PLB subsequently excluded PI – a direct indication that their PM resealed during the 4 h assay period (*Figure 6C and Video 11*). As expected, cells that were already permeable to SYTOX Green at the beginning of the incubation (likely non-viable cells that were damaged prior to the incubation) were also permeable to PI (which causes strong quenching of the SYTOX green fluorescence upon entering cells - *Figure 6C and Video 11*). Interestingly, primary B-cells permeabilized during interaction with αM-beads (*Figure 1A and Video 1*) or αM-PLB (*Figure 1H, Figure 6C and Video 11*) often displayed a shape change visualized as an increase in cell diameter, but after resealing this morphological change was gradually reversed (Figure 6C, Figure 6-figure supplement 2, Videos 11 and 12). Collectively,

our results indicate that B-cell PM permeabilization by binding to surface-associated antigen is a reversible event, and that lysosomal exocytosis is required for PM resealing as previously shown for other cell types (Andrews *et al.* 2014).

B-cell permeabilization and lysosomal exocytosis facilitate internalization and presentation of surface-associated antigen

We investigated the relationship between PM permeabilization by surface-associated antigen and antigen internalization using fluorescent αM covalently bound to beads or tethered to PLB. Live imaging detected αM puncta moving away from bead-binding sites into B-cells, increasing progressively between 30 and 60 min of interaction (*Figure 7A and B and Video 13*). In contrast, intracellular fluorescent puncta were markedly less abundant during the same time period in cells not binding αM-beads, or binding Tf-beads (*Figure 7B*). Inhibition of antigen-mediated PM permeabilization with blebbistatin significantly reduced extraction and internalization of αM coupled to beads (*Figure 7C*). When similar experiments were performed with PLB, the fraction of cells containing internalized αM and the total amount of αM uptake were significantly higher in permeabilized cells with high levels of intracellular FM staining (FM-high), compared to non-permeabilized cells with low FM staining (FM-low) (*Figure 7D-F*). These data suggest that αM-induced PM permeabilization, rapidly followed by lysosomal exocytosis, promotes extraction and internalization of αM from non-internalizable surfaces.

Next, we investigated whether antigen internalization enhanced by PM permeabilization and lysosomal exocytosis impacts antigen presentation by B-cells. We compared levels of IL-2 secretion by the 3A9 T-cell hybridoma line (Allen and Unanue 1984) after activation by B-cells

exposed to HEL- or DEL-I-beads. B-cells exposed to high concentrations of soluble HEL or DEL-I induced similar levels of IL-2 secretion (*Figure 7G*), demonstrating that the primary B-cells used in these assays could process and present the conserved peptide present in both HEL and DEL-I for T-cell activation. In contrast, when the B-cells were exposed to lower amounts of surface-associated antigens, B-cells exposed to HEL-beads activated T-cells to produce IL-2 at markedly higher levels than cells exposed to DEL-I-beads *(Figure 7H*). These results indicate that B-cell permeabilization resulting from high-affinity antigen-BCR interaction, with its corresponding lysosomal exocytosis response, facilitates the presentation of antigen associated with non-internalizable surfaces.

Discussion

Extracellular release of lysosomal enzymes by B-cells was previously proposed to cleave antigens tightly associated with non-internalizable surfaces, facilitating internalization and presentation to T-cells (Yuseff *et al.* 2011; Spillane and Tolar 2017). However, it was unclear which mechanism was responsible for inducing lysosomal enzyme release when B-cells engaged insoluble antigen. In this study, we show that interaction of the BCR with surface-associated antigen can permeabilize the B-cell PM, triggering lysosomal exocytosis as part of the PM repair response (Rodríguez *et al.* 1997; Reddy *et al.* 2001). Antigen-dependent PM permeabilization occurs at antigen-binding sites and is reversible under conditions that allow lysosomal exocytosis. We further demonstrate that PM permeabilization and lysosomal exocytosis require high-affinity binding of the BCR to antigen, BCR signaling and activation of NMII motor activity, and that this process facilitates antigen internalization, processing, and presentation. Thus, our study identifies a critical novel step in the affinity-dependent process by which B-cells

311 capture antigen tightly associated with surfaces, for effective internalization and subsequent
312 presentation to T-cells.
313
314 Capture and internalization of antigen tightly associated with surfaces is an important
315 immunological process, as B-cells encounter this type of antigen *in vivo* on parasites, bacteria
316 and viruses, as well as immune cells such as follicular dendritic cells. Follicular dendritic cells
317 capture antigen drained into lymph nodes and present it on their surface to germinal center B-
318 cells. In this manner, follicular dendritic cells enhance BCR antigenic stimulation by increasing
319 antigen avidity, in addition to providing costimulatory molecules (Natarajan *et al.* 2001). While
320 the exact percentage is unknown, studies have suggested that the majority of antigens that B-
321 cells encounter *in vivo* are in a membrane-associated form (Batista and Harwood 2009).
322 Importantly, the capture, internalization, and presentation of such surface-associated antigens to
323 T-cells play a critical role in selecting specific B-cells for survival, clonal expansion and
324 differentiation into long-lived high-affinity memory B-cells and antibody-secreting cells (Gitlin
325 *et al.* 2014).
326
327 We found that B-cell PM permeabilization induced by surface-associated antigen depends on the
328 motor activity of NMII. Following BCR polarization, activated NMII accumulates at sites of B-
329 cell binding to αM- or HEL-beads or PLB before permeabilization occurs. These findings are
330 consistent with previous studies showing that internalization of surface-associated but not
331 soluble antigen requires NMII-mediated traction forces at antigen-binding sites (Natkanski *et al.*
332 2013; Spillane and Tolar 2018). Collectively, our results support the notion that NMII-mediated
333 traction forces generated during BCR-antigen interaction are responsible for permeabilization of

the B-cell PM. Whether this permeabilization is due to tearing of the lipid bilayer (Andrews *et al.* 2014) or the opening of mechanosensitive membrane channels (Liu *et al.* 2018; Liu and Ganguly 2019) is currently unknown. However, our finding that three distinct membrane-impermeable probes, PI, FM lipophilic dyes, and Ponceau 4R readily gain access to the cytosol after B-cell interaction with surface-associated antigen suggest that NMII-mediated membrane tearing is the mechanism underlying antigen-dependent B-cell PM permeabilization. In this context, it is noteworthy that Endophilin A2, a protein that facilitates the resealing of PM wounds (Corrotte *et al.* 2020), also contributes to BCR-mediated internalization of membrane-associated antigen (Malinova *et al.* 2021).

We were initially surprised to observe B-cell PM permeabilization during BCR-mediated binding of surface-associated antigen, a process that is known to generate myosin-mediated forces as a mechanism to capture antigen. To confirm that permeabilization occurs, we utilized three different membrane-impermeable probes, two types of BCR ligands, and three types of presenting surfaces. All generated similar results. We first detected B-cell permeabilization during interaction with surface-associated antigen by following the entry of membrane-impermeable DNA-binding or lipophilic dyes. While these compounds bind to different intracellular structures, both showed sudden rather than gradual increases in intracellular staining, consistent with PM permeabilization. To strengthen these results, we designed an independent assay based on the ability of Ponceau 4R to enter B-cells and quench the fluorescence of CFSE, a widely used vital dye that covalently labels cytosolic molecules without affecting cell viability. Ponceau 4R has been used to reduce the extracellular background of fluorescence-based assays because it is membrane-impermeable and potently quenches the

357 emission of fluorophores in the 490-560 nm range (Tay *et al.* 2019). We found that Ponceau 4R
358 influx rapidly quenches the fluorescence of CFSE-labeled B-cells, providing us with an
359 independent and accurate tool to determine the kinetics of antigen-induced PM permeabilization.
360 We also showed that endocytosis does not account for the sudden, massive influx of lipophilic
361 dyes that occurs in B-cells binding surface-associated antigen. Cross-linking surface BCRs with
362 soluble antibodies (Song *et al.* 1995; Cousin *et al.* 2018), which did not permeabilize the B-cell
363 PM, induced the endocytosis of lipophilic dyes - as expected from a tracer that is associated with
364 the outer leaflet of the PM. However, the endocytosed lipophilic dye appeared as small puncta
365 that gradually accumulated at the cell periphery, in sharp contrast to the sudden, massive dye
366 influx that reaches the nuclear envelope in antigen-permeabilized cells. Consistent with this
367 result, endocytosed fluorescent Fab' covalently attached to beads also appeared as small puncta
368 in our live imaging assays. Thus, we conclude that the sudden, massive influx of lipophilic dyes
369 is the result of PM permeabilization but not of dye endocytosis.
370
371 The PM of primary B-cells can be damaged by phototoxicity during prolonged live imaging, or
372 by necrosis or apoptosis. To control for such events, in parallel to our assays with surface-
373 associated antigen, we measured the permeabilization levels of cells interacting with Tf-beads or
374 Tf-PLB, which bind the Tf receptor with similar affinity as antigen-BCR but without BCR
375 activation (Fuchs and Gessner 2002). Low levels of non-specific permeabilization of B-cells
376 could be detected in all our assays, not surprisingly given that primary splenic B-cells are often
377 injured during the purification process. Furthermore, we did not observe an increase in apoptotic
378 markers in B-cells interacting with surface-associated antigen. Importantly, our assays involving
379 sequential exposure to membrane-impermeable dyes revealed that a significant fraction of the

antigen-permeabilized B-cells subsequently resealed. Thus, our findings cannot be explained by a loss in B-cell viability, strongly suggesting that B-cells can become transiently permeabilized when binding antigen that is tightly associated with surfaces.

We found that two different model antigens, αM and HEL, can induce B-cell PM permeabilization when attached to surfaces. This shows that BCR binding through *bona fide* antigen-binding sites is not a requirement for generation of the mechanical forces leading to B-cell PM permeabilization. Since stiffness of the antigen-presenting surface appears to impact BCR signaling and antigen capture (Spillane and Tolar 2017; J. Wang *et al.* 2018), it could be argued that antigen tethered to latex beads or PLB assembled on glass coverslips represent unnaturally stiff surfaces that might cause B-cell permeabilization. To investigate this issue, we utilized COS-7 cells expressing mHEL, a surface-associated antigen previously shown to engage MD4 B-cells *in vivo* when expressed in mouse models (Hartley *et al.* 1991). Our finding that BCR engagement of mHEL on the surface of COS-7 cells also induces PM permeabilization supports the notion that this process occurs under physiological conditions and is likely to be relevant *in vivo*.

Not all B-cells binding surface-associated antigen were permeabilized, possibly due to heterogeneity of the primary B-cell population used in our assays. Splenic B-cells are found at different stages of peripheral maturation and differentiation (Sagaert and De Wolf-Peeters 2003; Allman and Pillai 2008), binding antigen with variable affinities at different times and generating distinct responses. In subsequent studies, it will be interesting to determine which subsets of B-

cells are more effective in capturing and presenting surface-associated antigen through NMII-dependent PM permeabilization.

The rapid exocytosis of lysosomes triggered by B-cell permeabilization uncovered in our study provides a mechanistic explanation for the previously reported affinity-dependent extraction and presentation of antigen associated with non-internalizable surfaces (Batista and Neuberger 2000). We showed that the low affinity DEL-I antigen induces markedly lower levels of PM permeabilization, lysosome exocytosis, and antigen presentation when compared to the higher affinity HEL, when the two antigens are displayed on surfaces at similar densities. Surface association significantly enhances the avidity of antigens by increasing their valency, a process that can reduce the impact of BCR-binding affinity on BCR signaling, antigen internalization, and presentation when compared to soluble forms of the same antigen. However, this avidity effect is primarily observed with antigen associated with surfaces that B-cells are able to internalize (Batista and Neuberger 2000), and it is known that B-cell subsets such as native follicular B-cells have very low phagocytic capacity (Vidard *et al.* 1996). We envision that when antigen is strongly associated with non-internalizable surfaces, low-affinity BCR-antigen interactions are disrupted before B-cells can extract antigen. In this scenario, high-affinity BCR interactions would be critical for sustaining antigen binding under NMII-mediated traction forces, to promote PM permeabilization, lysosomal enzyme release, and antigen extraction. High-affinity BCR-antigen binding is also expected to induce more robust signaling than low-affinity binding, enabling higher levels of NMII activation (Fleire *et al.* 2006; Natkanski *et al.* 2013) and polarization to drive PM permeabilization. Collectively, in addition to supporting the notion that tight antigen attachment to non-internalizable surfaces facilitates B-cell affinity

425 discrimination, our results expand the mechanistic understanding of why different physical and
426 chemical forms of immunogens impact the efficacy of vaccines (Bachmann and Jennings 2010;
427 Khan *et al.* 2015).
428
429 Lysosomal exocytosis is acutely dependent on rapid elevations in $[Ca^{2+}]_i$ (Reddy *et al.* 2001;
430 Jaiswal *et al.* 2002). PM tears cause immediate Ca^{2+} influx and massive lysosomal exocytosis
431 (Reddy *et al.* 2001, Tam *et al.* 2010), due to the markedly higher Ca^{2+} concentration in the
432 extracellular space compared to the cytoplasm. BCR engagement of antigen also induces $[Ca^{2+}]_i$
433 increases (Baba and Kurosaki 2016; Tanaka and Baba 2020), and we cannot rule out the
434 possibility that BCR-mediated Ca^{2+} fluxes might contribute to the initiation of lysosomal
435 exocytosis, which would then be amplified by PM permeabilization and more robust Ca^{2+} influx.
436 However, while BCR-induced Ca^{2+} fluxes occur in most antigen-binding B-cells within seconds
437 of antigen binding, we found that the majority of lysosomal exocytosis and antigen
438 internalization events occur >30 min after antigen binding, a time frame that coincides with the
439 period required for antigen-induced PM permeabilization. Thus, our data suggest that BCR-
440 mediated $[Ca^{2+}]_i$ increases are unlikely to be the primary driver of the lysosomal exocytosis
441 events that facilitate endocytosis of surface-associated antigen. However, BCR-triggered Ca^{2+}
442 fluxes may have induced the small number of initial lysosomal exocytosis events that we
443 detected during the first 15 min of B-cell interaction with surface-associated antigen. It is also
444 conceivable that early BCR-induced Ca^{2+} fluxes contribute to antigen-induced B-cell PM
445 permeabilization by activating NMII and actin reorganization (Izadi *et al.* 2018).
446

Collectively, our results provide important insights into the spatiotemporal relationship of events initiated by interaction of the BCR with surface-associated antigen (*Figure 7I*). Our findings suggest that high-affinity binding stabilizes BCR-antigen interactions, inducing strong BCR signaling and NMII activation to locally generate traction forces that permeabilize the PM. Ca^{2+} entry would then trigger a localized PM repair response mediated by lysosomal exocytosis, releasing hydrolases that can cleave antigen off surfaces, facilitating endocytosis and presentation to T-cells. Our results support the notion that B-cells utilize a cellular mechanism that evolved for surviving PM injury to promote the acquisition, presentation, and possibly affinity discrimination of surface-associated antigens.

Materials and Methods

Key resources table

Reagent type (species) or resource	Designation	Source or reference	Identifiers	Additional information
Primary cell (spleen - C57BL/6)	WT	Jackson Laboratories	000664	
Primary cell (spleen -C57BL/6-Tg (IghelMD4)4Ccg/ J))	MD4	Jackson Laboratories	002595	
Primary cell (spleen B10.BR-$H2^{K2}$ H2-$T18^{a}$/ SgSnJJrep	B10.BR-$H2^{K2}$ H2-$T18^{a}$/ SgSnJJrep	Jackson Laboratories	004804	
Cell line (*Mus musculus*)	A20	ATCC	TIB-208	B-cell lymphoma
Cell line (*Mus musculus*)	3A9	ATCC	CRL-3293	T-cell hybridoma

Cell line (*Cercopithecus aethiops*)	COS-7	ATCC	CRL-1651	Kidney fibroblasts
Reagent	Latex NH_2-beads	Polysciences	17145-5	
Ligand	αM ($F(ab')_2$ goat-anti-mouse IgM+G)	Jackson Immune Research	115-006-068	Binds to BCR
Antigen	HEL (Hen egg lysozyme)	Sigma-Aldrich	L6876	Binds to BCR from MD4 mice
Antigen	DEL-1 (Duck egg lysozyme)	David B. Langley and Daniel Christ laboratory		Binds to BCR from MD4 mice
Ligand	Tf (Holo-transferrin)	Sigma-Aldrich	T0665-50MG	Binds to transferrin receptor
Ligand	AF488-αM	Jackson Immune Research	115-546-003	Binds to BCR
Ligand	AF488-Tf	Thermo Fisher Scientifc	T13342	Binds to transferrin receptor
Commercial kit	BCA kit	Thermo Fisher Scientific	23235	Protein measurement during bead preparation
Control for antigen	Biotinylated transferrin (Tf-PLB)	Sigma-Aldrich	T3915-5MG	
Reagent	Streptavidin-conjugated Yellow-Green latex beads	Polysciences	24159-1	
Ligand	Biotin-SP (long spacer)-conjugated Fab fragments of goat-anti-mouse IgG	Jackson Immune Research	115-067-003	

	(H+L)			
Inhibitor	Bleb (Blebbistatin)	Sigma-Aldrich	B0560	50 µM
Antibody	anti-phosphotyrosine mAb 4G10	Millipore	05-321	1:500
Antibody	AF488-goat-anti-mouse IgG_{2b}	Thermo Fisher Scientific	A-21141	1:500
Reagent	PI (Propidium iodide)	Sigma-Aldrich	P4170-10MG	50 µg/ml
Reagent	FM1-43FX	Thermo Fisher Scientific	F35355	10 µg/ml
Reagent	FM4-64FX	Thermo Fisher Scientific	F34653	10 µg/ml
Reagent	SYTOX™ Blue	Invitrogen	S11348	300 nM
Reagent	SYTOX™ Green	Invitrogen	S7020	300 nM
Antibody	AF647 donkey-anti-goat IgG (H+L)	Invitrogen	A21447	10 µg/ml
Inhibitor	Staurosporine	Abcam	120056	Apoptosis induction (1 µM)
Antibody	Cleaved Caspase-3 (Asp175) Antibody	Cell Signaling	9661T	1:500
Antibody	Cy5-Fab donkey-anti mouse IgG	Jackson ImmunoResearch	715-175-151	5 µg/ml
Antibody	Donkey anti-Rabbit IgG (H+L) Highly cross-adsorbed secondary antibody, Alexa Fluor 488	Thermo Fisher Scientific	A-21206	1:200

Inhibitor	PP2	Millipore-Sigma	529573	Src kinase inhibitor (5 μM)
Inhibitor	AVL-292	Selleckchem	S7173	BTK inhibitor (10 nM)
Antibody	anti-BTK	Cell Signaling	8547	1:1000
Antibody	Rabbit anti-phospho-BTK	Abcam	68217	1:500
Antibody	HRP goat-anti-rabbit	Jackson Immune Research	111-035-144	1:1000
Antibody	Cy3-Fab donkey-anti–mouse IgM+G	Jackson Immune Research	115-165-166	1:200
Antibody	Rabbit anti-phosphorylated myosin light chain (pMLC)	Cell Signaling	3671S	1:50
Antibody	AF633-goat-anti-rabbit IgG	Invitrogen	A-21070	1:500
Inhibitor	BEL (Bromoenol lactone)	Sigma-Aldrich	B1552	12 μM
Commercial kit	SiR-Lysosome and Verapamil	Cytoskeleton	CY-SC012	Lysosome probe 1 μM and 10 μM
Antibody	Rabbit-anti-LIMP-2	Sigma-Aldrich	SAB3500449-100UG	1:200
Antibody	AF488 donkey-anti-rabbit IgG	Life technology	A32790	1:200
Commercial kit	IL-2 ELISA kit	Biolegend	431804	
Software	FlowJo 10.1	FlowJo, LLC		https://www.flowjo.com/solutions/flowjo/downloads
Software	Volocity Suite	PerkinElmer		https://ir.perkinelmer.com/news-releases/news-release-details/perkinelmer-launches-volocityr-60-high-

				performance-3d-cellular
Software	NIH Image J	NIH		https://imagej.nih.gov/ij/
Software	MATLAB	MathWorks		https://www.mathworks.com/products/matlab.html
Software	Prism	GraphPad		https://www.graphpad.com/scientific-software/prism/
Antibody	Anti-CD90.2	Biolegend	105310	1 µl/ $2x10^6$ cells
Reagent	Guinea pig complement	Innovative Research	IGGPCSER	100 µl/ $4x10^7$ cells
Reagent	1,2-dioleoyl-sn-glycero-3-phosphocholine	Avanti Polar Lipids	850375P	5 mM (PLB)
Reagent	1,2-dioleoyl-sn-glycero-3-phosphoethanolamine-cap-biotin	Avanti Polar Lipids	870273C	50 µM (PLB)
Reagent	Ponceau 4R	Sigma-Aldrich	18137	1 mM
Reagent	CFSE	Thermo Fisher Scientific	C34553	1 µM
Reagent	Lipofectamine 3000	Thermo Fisher Scientific	L3000008	
Reagent	Bovine fibronectin	Millipore	341631	5 mg/ml

Mice, B-cell isolation and culture

Primary B-cells were isolated from the spleens of wild type C57BL/6, MD4 transgenic (C57BL/6 background), B10.BR-*H2*^{k2} *H2-T18*^{a}/SgSnJJrep (Jackson Laboratories), and F1 of B10.BR-*H2*^{k2} *H2-T18*^{a}/SgSnJJrep x MD4 mice using a previously published protocol (Miller *et al.* 2015). Briefly, mononuclear cells were isolated by Ficoll density-gradient centrifugation

(Sigma-Aldrich). T-cells were removed with anti-mouse CD90.2 mAb (BD Biosciences) and guinea pig complement (Innovative Research, Inc.) and monocytes and dendritic cells by panning. B-cells were kept at 37°C and 5% CO_2 before and during experiments. All procedures involving mice were approved by the Institutional Animal Care and Usage Committee of the University of Maryland.

The A20 B-cell lymphoma line (ATCC #TIB-208) was cultured in DMEM (Lonza) supplemented with 10% of FBS (Thermo Fisher Scientific), 0.05 mM 2-mercaptoethanol (Sigma-Aldrich), 10 mM MOPS, 100 units/ml penicillin, and 100 µg/ml streptomycin (Gemini) at 37°C and 5% CO_2. The 3A9 T-cell hybridoma line (ATCC #CRL-3293) was cultured in DMEM (ATCC) supplemented with 5% FBS (Thermo Fisher Scientific), 0.05 mM 2-mercaptoethanol (Sigma-Aldrich) at 37°C and 5% CO_2.

Antigen-coated beads

Latex NH_2-beads (3 µm diameter, 3.5 x 10^8 beads/preparation, Polysciences) were activated with 8% glutaraldehyde in 0.5 ml PBS for 120 min under rotation at room temperature, washed with PBS, and incubated overnight with equal molar amounts of F(ab')$_2$ goat-anti-mouse IgM+G (αM, 20 µg/ml, Jackson ImmunoResearch Laboratories), hen egg lysozyme (HEL, 5.8 µg/ml, Sigma-Aldrich), duck egg lysozyme (DEL)-I (Langley *et al.* 2017), holo-transferrin (Tf, 32 µg/ml, Sigma-Aldrich), Alexa Fluor (AF) 488-conjugated Tf (AF488-Tf, 32 µg/ml, Thermo Fisher Scientific), or AF488-F(ab')$_2$ goat-anti-mouse IgM+G (AF488-αM, 20 µg/ml, Jackson ImmunoResearch Laboratories) in 1 ml PBS. Protein content determination (BCA, Thermo Fisher Scientific) of coupling solutions before and after bead incubation confirmed that similar molar amounts of protein were conjugated in each case. The beads were then blocked with PBS

1% BSA for 30 min under rotation, washed to remove unconjugated proteins, counted in a Neubauer chamber and stored at 4°C in PBS containing 1% BSA and 5% glycerol. Streptavidin-conjugated Yellow-Green latex beads (2 μm diameter, 5 x 10^8 beads/preparation, Polysciences) were washed with 1% BSA in PBS and incubated with Biotin-SP (long spacer)-conjugated Fab fragments of goat-anti-mouse IgG (H+L) (40 μg of biotinylated antibody/mg of beads, Jackson ImmunoResearch Laboratories) for 30 min at 4°C, washed, counted in a Neubauer chamber and stored at 4°C in PBS containing 1% BSA and 5% glycerol.

Antigen-coated planar lipid bilayers (PLB)

PLB were prepared as previously described (Dustin *et al.* 2007; Liu *et al.* 2012; Spillane and Tolar 2017). Briefly, liposomes were generated from 5 mM 1,2-dioleoyl-sn-glycero-3-phosphocholine plus 1,2-dioleoyl-sn-glycero-3-phosphoethanolamine-cap-biotin (Avanti Polar Lipids) at a 100:1 molar ratio by sonication. Eight-well coverslip chambers (Lab-Tek) were incubated with liposomes for 20 min at room temperature and washed with PBS. The chambers were then incubated with 1 μg/ml streptavidin (Jackson ImmunoResearch Laboratories) for 10 min, washed, and incubated with 10 μg/ml mono-biotinylated Fab' goat-anti-IgM+G (αM-PLB) (Liu *et al.* 2012) or the same molar amount of biotinylated Tf (16 μg/ml, Sigma-Aldrich) (Tf-PLB) for 10 min at room temperature.

COS-7 cells expressing membrane hen egg lysozyme-GFP (mHEL-GFP)

COS-7 cells were transiently transfected with mHEL-GFP (Batista *et al.* 2001) (plasmid kindly provided by Dr. Michael Gold, University of British Columbia) using Lipofectamine 3000

(Thermo Fisher Scientific) and a published protocol (J.C. Wang *et al.* 2018), and used for experiments 24 h post-transfection.

Flow cytometry analysis of PM permeabilization

Mouse splenic B-cells were incubated with beads coated with αM, HEL, DEL-I or Tf in DMEM containing 6 mg/ml BSA (DMEM-BSA) at a cell:bead ratio of 1:2 (or as indicated), or with soluble F(ab')$_2$ goat-anti-mouse IgM+G (sαM, 0.5 μg/ml) for 30 min at 37°C with 5% CO_2. Propidium iodide (PI, Sigma-Aldrich) was present during the 37°C incubation as an indicator of PM permeabilization. Cells were then analyzed by flow cytometry (BD FACSCanto II) at 10,000 cell counts/sample. Bead-bound cells were identified based on their forward- (FSC) and side-scatter (SSC) properties and on fluorescence intensity (FI) when using fluorescent beads (*Figure 1-figure supplement 2*). The percentages of PI-positive (PI+) cells among the bead-bound cell populations were quantified using FlowJo 10.1 software.

Live cell imaging of PM permeabilization

To assess PM permeabilization by protein-coated beads, mouse splenic B-cells or a B-cell line (A20) were incubated for 30 min at 4°C in 35 mm glass-bottom dishes (MatTek) coated with poly-lysine and then with protein-coated beads at a cell:bead ratio of 1:2 for another 30 min at 4°C. Cells were washed with DMEM-BSA and imaged in a Live Cell System chamber (Pathology Devices) at 37°C with 5% CO_2 in the presence of 50 μg/ml PI (Sigma-Aldrich) with or without 50 μM blebbistatin (Sigma-Aldrich). Images were acquired for 60 min at 1 frame/15-30 s using a spinning disk confocal microscope (UltraVIEW VoX, PerkinElmer with a 63X 1.4

532 N.A. oil objective). Images were analyzed using Volocity Suite (PerkinElmer) and NIH ImageJ.
533 More than 200 cells from 3 independent experiments were analyzed for each condition.

534 To assess PM permeabilization after binding to ligand-coated PLB, splenic B-cells were
535 incubated with FM1-43FX or FM4-64FX (Thermo Fisher Scientific) in DMEM-BSA for 5 min
536 at 4^{o}C, added to coverslip chambers containing mono-biotinylated Fab' goat-anti-IgM+G or
537 biotinylated Tf tethered to PLB, and imaged immediately at 37°C with 5% CO_2 using a spinning
538 disk confocal microscope (UltraVIEW VoX, PerkinElmer with a 63X 1.4 N.A. oil objective)
539 with or without 50 μg/ml PI and/or 10 μg/ml FM1-43FX or FM4-64FX (Thermo Fisher
540 Scientific). Images were acquired at 1 frame/6-10 s and analyzed using Volocity (PerkinElmer)
541 and NIH ImageJ. For quantitative analysis, the mean fluorescence intensity (MFI) of FM1-43FX
542 or FM4-64FX in a defined area was measured using Volocity (PerkinElmer). More than 270
543 cells from 3 independent experiments were analyzed for each condition. For 4 h videos, DMEM
544 without phenol red containing 2% FBS was used, and images were acquired at 1 frame/30 s in
545 the presence of PI (50 μg/ml).

546 PM permeabilization was also assessed using Ponceau 4R-mediated quenching of a
547 cytosolic fluorescent dye. B-cells were pre-stained with 1 μM CFSE (Thermo Fisher Scientific)
548 for 10 min at 37^{o}C, washed with DMEM, incubated with αM- or Tf -PLB and analyzed in a
549 spinning disk confocal microscope (UltraVIEW VoX, PerkinElmer with a 40X 1.4 N.A. oil
550 objective) in the presence or absence of 1 mM Ponceau 4R (Sigma-Aldrich). More than 480 cells
551 from four independent experiments were analyzed for each condition. To validate this method,
552 cells pre-stained with CFSE were incubated with or without 800 ng/ml SLO in the presence or
553 absence of 1 mM Ponceau 4R (Sigma-Aldrich) for 10 min and analyzed by flow cytometry (BD
554 FACSCanto II) at 10,000 cell counts/sample.

To assess the ability of antigen exposed on the surface of mammalian cells to permeabilize B-cells, COS-7 cells mock-transfected or transfected with mHEL-GFP were seeded on fibronectin-coated coverslips and cultured for 24 h. WT or MD4 B-cells pre-stained with AF674-conjugated Fab fragments of donkey-anti–mouse IgM+G (Jackson ImmunoResearch Laboratories) were then added to the COS-7 cells in the presence of 50 µg/ml PI and imaged immediately at 37°C with 5% CO_2 using a spinning disk confocal microscope (UltraVIEW VoX, PerkinElmer with a 40X 1.3 N.A. oil objective). Images were acquired at 1 frame/20s and analyzed using NIH ImageJ software. More than 240 cells from 3 independent experiments were analyzed for each condition.

Cleaved caspase-3 detection

Splenic B-cells were pretreated or not with 1 µM staurosporine (Abcam) for 24 h at 37°C in DMEM-BSA to induce apoptosis (Diaz *et al.* 2004), exposed to αM- or Tf-beads for 30 min at 37°C, washed, fixed with 4% paraformaldehyde (PFA), blocked with 1% BSA, and permeabilized with 0.05% saponin. Cells were then incubated with antibodies specific for cleaved caspase-3 (Asp175) (Cell Signaling Technology) followed by AF488 donkey-anti-rabbit IgG (Life Technologies) and analyzed by flow cytometry (BD FACSCanto II) at 10,000 cell counts/sample. The percentages of cells with cleaved caspase-3 staining were determined using FlowJo 10.1 software.

BCR signaling

BCR signaling was analyzed using both flow cytometry and western blotting. For flow cytometry assays, splenic B-cells from MD4 mice were pretreated or not with 5 µM of the Src

kinase inhibitor PP2 (Millipore) (Cheng *et al.* 2001) for 30 min at 37°C (conditions selected not to cause B-cell toxicity) and then incubated with HEL-beads in the presence or not of the inhibitor at 37°C for 30 min. Cells were fixed with 4% PFA, permeabilized with 0.05% saponin, incubated with mouse anti-phosphotyrosine mAb (4G10, Millipore) followed by AF488-goat-anti-mouse IgG_{2b} (Thermo Fisher Scientific) secondary antibodies, and analyzed by flow cytometry (BD FACSCanto II) at 10,000 cell counts/sample. The data were analyzed using FlowJo 10.1 software.

For western blot assays, splenic B-cells from MD4 mice were pretreated or not with 10 nM of the BTK inhibitor AVL-292 (Selleckchem) (Aalipour and Advani 2013) for 30 min at 37°C (conditions selected not to cause B-cell toxicity) and incubated with HEL-beads in the presence or not of the inhibitor at 37°C for 30 min. Cells were then lysed using RIPA buffer (150 mM $NaCl_2$, 1% of NP40, 0.5% Sodium deoxycholate, 0.1% SDS, 50 mM Tris, pH 8.0) containing protease and phosphatase inhibitors (50 mM NaF, 1 mM Na_3VO_4 and 10 mM $Na_4P_2O_7$) at 4°C. Cell lysates were run in 4-20% gradient SDS-PAGE gels (Bio-Rad) ($5x10^6$ cells/ lane) and transferred (Bio-Rad Trans-Blot transfer system) to PVDF membranes (Millipore). The membranes were blotted with rabbit anti-phospho-BTK (pBTK; Abcam) or anti-BTK (Cell Signaling Technology) followed by HRP-anti-rabbit antibodies (Jackson ImmunoResearch Laboratories) and visualization using ECL substrate (Bio-Rad) and imaging (iBright FL-1500, (Thermo Fisher Scientific).

To check if signaling affected PM permeabilization, splenic B-cells from MD4 mice were pretreated or not with 5 μM PP2 (Cheng *et al.* 2001) or 10 nM AVL-292 (Aalipour and Advani 2013) for 30 min at 37°C and then incubated with HEL-beads in the presence or not of the

inhibitor and 50 μg/ml PI (Sigma-Aldrich) at 37°C for 30 min. The percentage of PI+ cells was expressed relative to the untreated condition.

BCR and NMII polarization

BCRs on the surface of mouse splenic B-cells were stained with Cy3-Fab donkey-anti–mouse IgM+G (Jackson ImmunoResearch Laboratories) for 30 min at 4°C. Cells were then incubated with αM- or Tf-beads at 4°C for 30 min and 37°C for different lengths of time. Cells were fixed with 4% PFA, permeabilized with 0.05% saponin, and incubated with rabbit anti-phosphorylated myosin light chain 2 (pMLC2) antibodies (Cell Signaling Technology) to label activated NMII (Bresnick 1999), followed by AF633-goat-anti-rabbit IgG (Invitrogen). Cells were analyzed by confocal fluorescence microscopy (Zeiss LSM710 with a 63X 1.4 N.A. oil objective). The percentages of cells with polarization of surface labeled BCRs and activated NMII towards bead-binding sites were quantified by visual inspection. More than 300 cells from 3 independent experiments were analyzed for each condition.

PM repair assays

Mouse splenic B-cells were pretreated or not with 12 μM bromoenol lactone (BEL, Sigma-Aldrich) in DMEM-BSA for 30 min at 37^{o}C before and during assays, to inhibit lysosomal exocytosis and PM repair (Fensome-Green *et al.* 2007). Cells were then incubated with αM-beads (1:2 cell:bead ratio) with or without inhibitors at 4^{o}C for 5 min and 37°C for 30 min in the presence of FM4-64FX (Thermo Fisher Scientific) to stain wounded cells. Cells were then incubated with SYTOX^{TM} Blue nucleic acid stain (300 nM, Invitrogen) at 4^{o}C for 10 min to stain cells that failed to repair PM wounds during the 30 min incubation. Cells were analyzed by

623 flow cytometry (BD FACSCanto II) at 10,000 cell counts/sample. Cells that were FM4-64FX
624 positive but SYTOX Blue negative were identified as permeabilized cells that resealed. The
625 percentages of resealed cells among all bead-bound permeabilized cells were quantified using
626 FlowJo 10.1 software.

627 To assess the resealing capacity of B-cells permeabilized by ligand-coated PLB using live
628 cell imaging, splenic B-cells were incubated with SYTOX Green (Thermo Fisher Scientific) in
629 DMEM-BSA for 5 min at 4^{o}C and added to coverslip chambers containing mono-biotinylated
630 Fab' goat-anti-IgM+G or biotinylated Tf tethered to PLB. Cells were imaged at 1 frame/30 s for
631 4 h at 37°C with 5% CO_2 using a spinning disk confocal microscope (UltraVIEW VoX,
632 PerkinElmer with a 63X 1.4 N.A. oil objective), followed by addition of 50 μg/ml PI (Thermo
633 Fisher Scientific) at the end of the assay and final image acquisition.
634
635 **BCR polarization in relation to permeabilization**
636 Surface BCRs of splenic B-cells were labeled with Cy5-Fab donkey-anti mouse IgG (Jackson
637 ImmunoResearch) at 4^{o}C for 30 min. Cells were incubated with αM-PLB in the presence of FM
638 4-64FX (Thermo Fisher Scientific) and imaged immediately at 37°C with 5% CO_2 using a
639 spinning disk confocal microscope (UltraVIEW VoX, PerkinElmer with a 60X 1.4 N.A. oil
640 objective). Images were acquired at 1 frame/20 s for 60 min and analyzed using a custom-made
641 MATLAB script (MathWorks) and NIH ImageJ software. BCR polarization was analyzed using
642 maximal projection of XZ images and quantified by the MFI ratio between defined regions
643 within the bottom half (closer to PLB) and the top half (away from PLB) of individual cells.
644 Cells with bottom to top ratios ≥2 were considered polarized. More than 20 cells from 3
645 independent experiments were analyzed.

646

647 **Lysosome exocytosis**

648 To detect LIMP-2 exposed on the cell surface, splenic B-cells (C57BL/6 or MD4) were
649 incubated with αM-, HEL-, DEL-I or Tf-beads for 30 min at 37°C, cooled to 4°C, and incubated
650 with rabbit-anti-LIMP-2 antibodies (Sigma-Aldrich) for 60 min at 4°C. Cells were then washed
651 and fixed with 4% PFA, washed, blocked with 1% BSA in PBS and incubated with AF488
652 donkey-anti-rabbit IgG (Life Technologies) secondary antibodies. For intracellular LIMP-2
653 staining, B-cells were fixed with 4% PFA, washed, permeabilized with 0.05% saponin for 20
654 min, and incubated with rabbit anti-LIMP-2 antibodies followed by AF488 donkey-anti-rabbit
655 IgG. Flow cytometry (BD FACSCanto II) was performed at 10,000 cell counts/sample. Cells
656 were also analyzed by confocal fluorescence microscopy (Leica SPX5 with a 63X 1.4 N.A. oil
657 objective). Polarization of LIMP-2 towards bound beads was quantified by calculating the
658 fluorescence intensity ratio (FIR) of anti-LIMP-2 at the B-cell-bead contact site relative to the
659 opposite side of the cell PM, using NIH ImageJ and a custom-made MATLAB script
660 (MathWorks).

661 Individual events of lysosome exocytosis were captured using total internal reflection
662 fluorescence (TIRF). Splenic B-cells were preloaded with SiR-Lysosome (1 μM, Cytoskeleton)
663 in the presence of verapamil (10 μM, Cytoskeleton) for 30 min at 37^{o}C. Cells were added to
664 coverslip chambers containing mono-biotinylated Fab' goat anti-IgM+G tethered to PLB and
665 imaged at 37°C with 5% CO_2 in the presence of PI (50 μg/ml, Sigma-Aldrich) using a TIRF
666 microscope (NIKON Eclipse Ti-E TIRF, 63X 1.49NA oil objective). Images were acquired at 8
667 frames/s during 15-20 min intervals of the 45 min incubation and analyzed using NIH ImageJ
668 and Nikon NIS Elements software. Increases in the FI of individual SiR-Lysosome puncta

(reflecting lysosome movement within the TIRF evanescent field towards the PM in contact with PLB) followed by sharp decreases within a period of 1-2 s (corresponding to a loss of the SiR-Lysosome signal upon PM fusion) were scored as exocytosis events (Jaiswal *et al.* 2002). More than 20 cells were analyzed in 4 independent experiments.

FM endocytosis after BCR crosslinking.

Mouse splenic B-cells were incubated with F(ab')$_2$ goat-anti-mouse IgM+G (10 µg/ml, Jackson ImmunoResearch Laboratories) for 10 min, followed by AF674-conjugated donkey-anti-goat (10 µg/ml, Invitrogen) for 30 min at 4^{o}C in coverslip chambers, to label and crosslink surface BCRs. FM1-43FX (10 µg/ml, Thermo Fisher Scientific) was added at the last 5 min of the 30 min incubation at 4^{o}C. Cells were washed and imaged at 37°C with 5% CO_2 in the presence of 50 µg/ml PI and 10 µg/ml FM1-43FX using a spinning disk confocal microscope (UltraVIEW VoX, PerkinElmer with a 63X 1.4 N.A. oil objective). Images were acquired at 1 frame/30 s for 60 min and analyzed using Volocity (PerkinElmer).

Assessment of BEL toxicity

Mouse splenic B-cells were pre-treated or not with 12 µM bromoenol lactone (BEL, Sigma-Aldrich) in DMEM-BSA for 30 min at 37^{o}C and then incubated with Tf-beads (1:2 cell-bead ratio) with or without the inhibitors at 37°C for 30 min in the presence of SYTOX^{TM} Blue (300 nM, Invitrogen). Cells were analyzed by flow cytometry (BD FACSCanto II) at 10,000 cell counts/sample. Bead-bound cells and SYTOX Blue positive cells were gated. The percentages of SYTOX Blue positive cells among all bead-bound permeabilized cells were quantified using FlowJo 10.1 software.

692

693 **Antigen internalization**

694 For live imaging of antigen internalization, splenic B-cells were incubated with AF488-αM-
695 beads (1:4 cell:bead ratio) in the presence of 1 μM SiR-Lysosome and 10 μM verapamil for 30
696 min at 4°C, washed with DMEM-BSA and imaged by confocal fluorescence microscopy (Leica
697 SPX5 with a 63X 1.4 N.A. oil objective) for 60 min at 1 frame/min at 37°C. Live time-lapse
698 images were analyzed using NIH ImageJ.

699 For fixed cell imaging, splenic B-cells were pretreated or not with 50 μM blebbistatin on
700 poly-lysine coated slides for 30 min at 4°C and incubated with AF488-αM beads or AF488-Tf-
701 beads at 37°C for varying lengths of time in the presence or not of 50 μM blebbistatin. After
702 fixation with 4% PFA, cells were imaged by confocal fluorescence microscopy (Zeiss LSM710
703 with a 63X 1.4 N.A. oil objective). Percentages of cells with intracellularly-located AF488-αM
704 puncta were determined by visual inspection of images. More than 200 cells from 3 independent
705 experiments were analyzed for each condition.

706 For live imaging of B-cells interacting with PLB, mouse splenic B-cells were added to
707 coverslip chambers containing PLB coated with AF488-conjugated mono-biotinylated Fab' goat-
708 anti-mouse IgM+G and incubated at 37°C with 5% CO_2 in the presence of 10 μg/ml FM 4-64FX
709 (Thermo Fisher Scientific) for varying lengths of time. Samples were then moved to 4°C for 5
710 min and immediately imaged using a confocal microscope (Leica SPX5 with a 63X 1.4 N.A. oil
711 objective). Internalization of antigen was quantified by determining the percentages of cells with
712 intracellularly-located AF488-Fab' goat-anti-mouse IgM+G puncta in each field and by
713 measuring the AF488 FI associated with intracellular puncta in individual cells, using a custom-
714 made MATLAB (MathWorks) script. Cells with high FM staining were identified as wounded

and those with low FM staining as unwounded. More than 15 fields or ~90 cells from 3 independent experiments (high or low FM staining) were analyzed for each condition.

Antigen presentation and T-cell activation

To detect antigen presentation to T-cells, splenic B-cells from F1 mice of a crossing between B10.BR-*H2*^{k2} *H2-T18*^{a}/SgSnJJrep and MD4 mice were co-cultured with 3A9 T-cell hybridoma cells (ATCC® CRL-3293™) at equal concentrations (3.75x10^{6} cells/ml). Cells were incubated in DMEM supplemented with 5% FBS and 0.05 mM 2-mercaptoethanol for 72 h in the presence or not of soluble HEL or DEL-I (10 µg/ml), or of beads coated with HEL, DEL-I or Tf (1:4 cell: bead ratio). After incubation, the concentration of IL-2 in the supernatant was measured using an IL-2 ELISA kit (Biolegend).

Statistical analysis

Statistical significance was assessed using unpaired, two-tailed Student's *t*-tests (Prism - GraphPad software) when only two groups were compared, and one-way ANOVA (parametric) or Kruskal-Wallis (non-parametric) when 3 or more groups were compared. All data were presented as the mean ± SD (standard deviation).

Acknowledgments

We thank Dr. A. Upadhyaya (Department of Physics, University of Maryland) for TIRF microscopy equipment and advice, A. Beaven (CBMG Imaging Core, University of Maryland) and K. Class (CBMG Flow Cytometry Core, University of Maryland) for assistance with confocal microscopy and flow cytometry, Drs. S. K. Pierce and M. Akkaya (NIH) for the 3A9 T-

cell hybridoma, Dr. B. Mittra and J. Jensen (University of Maryland) for SLO expression and purification, Dr. Michael Gold for providing the mHEL-GFP DNA construct, and members of the Song and Andrews laboratories for helpful discussions. This work was supported by the NIH grant R01 GM064625 to NWA and WS and NIH grant T32 GM080201 to JJHvH.

References

Aalipour, A. and Advani, R.H. (2013) 'Bruton tyrosine kinase inhibitors: a promising novel targeted treatment for B cell lymphomas', *Br J Haematol*, 163(4), 436-43, available: http://dx.doi.org/10.1111/bjh.12573.

Allen, P.M. and Unanue, E.R. (1984) 'Differential requirements for antigen processing by macrophages for lysozyme-specific T cell hybridomas', *J Immunol*, 132(3), 1077-9.

Allman, D. and Pillai, S. (2008) 'Peripheral B cell subsets', *Curr Opin Immunol*, 20(2), 149-57, available: http://dx.doi.org/10.1016/j.coi.2008.03.014.

Andrews, N.W., Almeida, P.E. and Corrotte, M. (2014) 'Damage control: cellular mechanisms of plasma membrane repair', *Trends in cell biology*, 24(12), 734-42, available: http://dx.doi.org/10.1016/j.tcb.2014.07.008.

Baba, Y. and Kurosaki, T. (2016) 'Role of Calcium Signaling in B Cell Activation and Biology', *Curr Top Microbiol Immunol*, 393, 143-74, available: http://dx.doi.org/10.1007/82_2015_477.

Bachmann, M.F. and Jennings, G.T. (2010) 'Vaccine delivery: a matter of size, geometry, kinetics and molecular patterns', *Nat Rev Immunol*, 10(11), 787-96, available: http://dx.doi.org/10.1038/nri2868.

759 Bansal, D., Miyake, K., Vogel, S.S., Groh, S., Chen, C.C., Williamson, R., McNeil, P.L. and
760 Campbell, K.P. (2003) 'Defective membrane repair in dysferlin-deficient muscular dystrophy',
761 *Nature*, 423(6936), 168-72, available: http://dx.doi.org/10.1038/nature01573.

762 Batista, F.D. and Harwood, N.E. (2009) 'The who, how and where of antigen presentation to B
763 cells', *Nat Rev Immunol*, 9(1), 15-27, available: http://dx.doi.org/10.1038/nri2454.

764 Batista, F.D., Iber, D. and Neuberger, M.S. (2001) 'B cells acquire antigen from target cells after
765 synapse formation', *Nature*, 411(6836), 489-94, available: http://dx.doi.org/10.1038/35078099.

766 Batista, F.D. and Neuberger, M.S. (1998) 'Affinity dependence of the B cell response to antigen:
767 a threshold, a ceiling, and the importance of off-rate', *Immunity*, 8(6), 751-9.

768 Batista, F.D. and Neuberger, M.S. (2000) 'B cells extract and present immobilized antigen:
769 implications for affinity discrimination', *EMBO J*, 19(4), 513-20, available:
770 http://dx.doi.org/10.1093/emboj/19.4.513.

771 Bresnick, A.R. (1999) 'Molecular mechanisms of nonmuscle myosin-II regulation', *Curr Opin*
772 *Cell Biol*, 11(1), 26-33.

773 Cheng, P.C., Brown, B.K., Song, W. and Pierce, S.K. (2001) 'Translocation of the B cell antigen
774 receptor into lipid rafts reveals a novel step in signaling', *J Immunol*, 166(6), 3693-701.

775 Corrotte, M., Cerasoli, M., Maeda, F.Y. and Andrews, N.W. (2020) 'Endophilin-A2-dependent
776 tubular endocytosis promotes plasma membrane repair and parasite invasion', *J Cell Sci*, 134(5),
777 available: http://dx.doi.org/10.1242/jcs.249524.

778 Cousin, M.A., Gordon, S.L. and Smillie, K.J. (2018) 'Using FM Dyes to Monitor Clathrin-
779 Mediated Endocytosis in Primary Neuronal Culture', *Methods Mol Biol*, 1847, 239-249,
780 available: http://dx.doi.org/10.1007/978-1-4939-8719-1_18.

781 Cyster, J.G. (2010) 'B cell follicles and antigen encounters of the third kind', *Nat Immunol*,
782 11(11), 989-96, available: http://dx.doi.org/10.1038/ni.1946.

783 Demonbreun, A.R., Fallon, K.S., Oosterbaan, C.C., Bogdanovic, E., Warner, J.L., Sell, J.J.,
784 Page, P.G., Quattrocelli, M., Barefield, D.Y. and McNally, E.M. (2019) 'Recombinant annexin
785 A6 promotes membrane repair and protects against muscle injury', *J Clin Invest*, 129(11), 4657-
786 4670, available: http://dx.doi.org/10.1172/JCI128840.

787 Diaz, D., Prieto, A., Barcenilla, H., Monserrat, J., Prieto, P., Sánchez, M.A., Reyes, E.,
788 Hernandez-Fuentes, M.P., de la Hera, A., Orfao, A. and Alvarez-Mon, M. (2004) 'Loss of
789 lineage antigens is a common feature of apoptotic lymphocytes', *J Leukoc Biol*, 76(3), 609-15,
790 available: http://dx.doi.org/10.1189/jlb.0304171.

791 Dustin, M.L., Starr, T., Varma, R. and Thomas, V.K. (2007) 'Supported planar bilayers for study
792 of the immunological synapse', *Curr Protoc Immunol*, Chapter 18, Unit 18.13, available:
793 http://dx.doi.org/10.1002/0471142735.im1813s76.

794 Fensome-Green, A., Stannard, N., Li, M., Bolsover, S. and Cockcroft, S. (2007) 'Bromoenol
795 lactone, an inhibitor of Group V1A calcium-independent phospholipase A2 inhibits antigen-
796 stimulated mast cell exocytosis without blocking Ca2+ influx', *Cell Calcium*, 41(2), 145-53.

797 Fleire, S.J., Goldman, J.P., Carrasco, Y.R., Weber, M., Bray, D. and Batista, F.D. (2006) 'B cell
798 ligand discrimination through a spreading and contraction response', *Science*, 312(5774), 738-41,
799 available: http://dx.doi.org/10.1126/science.1123940.

800 Fuchs, H. and Gessner, R. (2002) 'Iodination significantly influences the binding of human
801 transferrin to the transferrin receptor', *Biochim Biophys Acta*, 1570(1), 19-26.

802 Gitlin, A.D., Shulman, Z. and Nussenzweig, M.C. (2014) 'Clonal selection in the germinal centre
803 by regulated proliferation and hypermutation', *Nature*, 509(7502), 637-40, available:
804 http://dx.doi.org/10.1038/nature13300.

805 Gonzalez, S.F., Degn, S.E., Pitcher, L.A., Woodruff, M., Heesters, B.A. and Carroll, M.C.
806 (2011) 'Trafficking of B cell antigen in lymph nodes', *Annu Rev Immunol*, 29, 215-33, available:
807 http://dx.doi.org/10.1146/annurev-immunol-031210-101255.

808 Hartley, S.B., Crosbie, J., Brink, R., Kantor, A.B., Basten, A. and Goodnow, C.C. (1991)
809 'Elimination from peripheral lymphoid tissues of self-reactive B lymphocytes recognizing
810 membrane-bound antigens', *Nature*, 353(6346), 765-9, available:
811 http://dx.doi.org/10.1038/353765a0.

812 Hoogeboom, R. and Tolar, P. (2016) 'Molecular Mechanisms of B Cell Antigen Gathering and
813 Endocytosis', *Curr Top Microbiol Immunol*, 393, 45-63, available:
814 http://dx.doi.org/10.1007/82_2015_476.

815 Ibata, K., Kono, M., Narumi, S., Motohashi, J., Kakegawa, W., Kohda, K. and Yuzaki, M.
816 (2019) 'Activity-Dependent Secretion of Synaptic Organizer Cbln1 from Lysosomes in Granule
817 Cell Axons', *Neuron*, 102(6), 1184-1198.e10, available:
818 http://dx.doi.org/10.1016/j.neuron.2019.03.044.

819 Izadi, M., Hou, W., Qualmann, B. and Kessels, M.M. (2018) 'Direct effects of Ca^{2+}/calmodulin
820 on actin filament formation, *Biochem Biophys Res Commun*, 506(2), 355-360, available:
821 http://dx.doi.org/10.1016/j.bbrc.2018.07.159.

822 Jaiswal, J.K., Andrews, N.W. and Simon, S.M. (2002) 'Membrane proximal lysosomes are the
823 major vesicles responsible for calcium-dependent exocytosis in nonsecretory cells', *J Cell Biol*,
824 159(4), 625-35, available: http://dx.doi.org/10.1083/jcb.200208154.

825 Khan, F., Porter, M., Schwenk, R., DeBot, M., Saudan, P. and Dutta, S. (2015) 'Head-to-Head
826 Comparison of Soluble vs. Qβ VLP Circumsporozoite Protein Vaccines Reveals Selective
827 Enhancement of NANP Repeat Responses', *PLoS One*, 10(11), e0142035, available:
828 http://dx.doi.org/10.1371/journal.pone.0142035.

829 Langley, D.B., Crossett, B., Schofield, P., Jackson, J., Zeraati, M., Maltby, D., Christie, M.,
830 Burnett, D., Brink, R., Goodnow, C. and Christ, D. (2017) 'Structural basis of antigen
831 recognition: crystal structure of duck egg lysozyme', *Acta Crystallogr D Struct Biol*, 73(Pt 11),
832 910-920, available: http://dx.doi.org/10.1107/S2059798317013730.

833 Liu, C., Miller, H., Orlowski, G., Hang, H., Upadhyaya, A. and Song, W. (2012) 'Actin
834 reorganization is required for the formation of polarized B cell receptor signalosomes in response
835 to both soluble and membrane-associated antigens', *J Immunol*, 188(7), 3237-46, available:
836 http://dx.doi.org/10.4049/jimmunol.1103065.

837 Liu, C.S.C. and Ganguly, D. (2019) 'Mechanical Cues for T Cell Activation: Role of Piezo1
838 Mechanosensors', *Crit Rev Immunol*, 39(1), 15-38, available:
839 http://dx.doi.org/10.1615/CritRevImmunol.2019029595.

840 Liu, C.S.C., Raychaudhuri, D., Paul, B., Chakrabarty, Y., Ghosh, A.R., Rahaman, O., Talukdar,
841 A. and Ganguly, D. (2018) 'Cutting Edge: Piezo1 Mechanosensors Optimize Human T Cell
842 Activation', *J Immunol*, 200(4), 1255-1260, available:
843 http://dx.doi.org/10.4049/jimmunol.1701118.

844 Malinova, D., Wasim, L., Newman, R., Martínez-Riaño, A., Engels, N. and Tolar, P. (2021)
845 'Endophilin A2 regulates B-cell endocytosis and is required for germinal center and humoral
846 responses', *EMBO Rep*, e51328, available: http://dx.doi.org/10.15252/embr.202051328.

847 McNeil, P.L., Miyake, K. and Vogel, S.S. (2003) 'The endomembrane requirement for cell
848 surface repair', *Proc Natl Acad Sci U S A*, 100(8), 4592-7, available:
849 http://dx.doi.org/10.1073/pnas.0736739100.

850 Miller, H., Castro-Gomes, T., Corrotte, M., Tam, C., Maugel, T.K., Andrews, N.W. and Song,
851 W. (2015) 'Lipid raft-dependent plasma membrane repair interferes with the activation of B
852 lymphocytes', *J Cell Biol*, 211(6), 1193-205, available: http://dx.doi.org/10.1083/jcb.201505030.

853 Naegeli, K.M., Hastie, E., Garde, A., Wang, Z., Keeley, D.P., Gordon, K.L., Pani, A.M., Kelley,
854 L.C., Morrissey, M.A., Chi, Q., Goldstein, B. and Sherwood, D.R. (2017) 'Cell Invasion In Vivo
855 via Rapid Exocytosis of a Transient Lysosome-Derived Membrane Domain', *Dev Cell*, 43(4),
856 403-417.e10, available: http://dx.doi.org/10.1016/j.devcel.2017.10.024.

857 Natarajan, K., Sahoo, N.C. and Rao, K.V. (2001) 'Signal thresholds and modular synergy during
858 expression of costimulatory molecules in B lymphocytes', *J Immunol*, 167(1), 114-22.

859 Natkanski, E., Lee, W.Y., Mistry, B., Casal, A., Molloy, J.E. and Tolar, P. (2013) 'B cells use
860 mechanical energy to discriminate antigen affinities', *Science*, 340(6140), 1587-90, available:
861 http://dx.doi.org/science.1237572 [pii]10.1126/science.1237572.

862 Reddy, A., Caler, E.V. and Andrews, N.W. (2001) 'Plasma membrane repair is mediated by
863 Ca(2+)-regulated exocytosis of lysosomes', *Cell*, 106(2), 157-69.

864 Reth, M. (1994) 'B cell antigen receptors', *Curr Opin Immunol*, 6(1), 3-8.

865 Rodríguez, A., Webster, P., Ortego, J. and Andrews, N.W. (1997) 'Lysosomes behave as Ca2+-
866 regulated exocytic vesicles in fibroblasts and epithelial cells', *J Cell Biol*, 137(1), 93-104.

867 Sagaert, X. and De Wolf-Peeters, C. (2003) 'Classification of B-cells according to their
868 differentiation status, their micro-anatomical localisation and their developmental lineage',
869 *Immunol Lett*, 90(2-3), 179-86, available: http://dx.doi.org/10.1016/j.imlet.2003.09.007.

870 Shlomchik, M.J. and Weisel, F. (2012) 'Germinal center selection and the development of
871 memory B and plasma cells', *Immunol Rev*, 247(1), 52-63, available:
872 http://dx.doi.org/10.1111/j.1600-065X.2012.01124.x.

873 Song, W., Cho, H., Cheng, P. and Pierce, S.K. (1995) 'Entry of B cell antigen receptor and
874 antigen into class II peptide-loading compartment is independent of receptor cross-linking', *J*
875 *Immunol*, 155(9), 4255-63.

876 Spillane, K.M. and Tolar, P. (2017) 'B cell antigen extraction is regulated by physical properties
877 of antigen-presenting cells', *J Cell Biol*, 216(1), 217-230, available:
878 http://dx.doi.org/10.1083/jcb.201607064.

879 Spillane, K.M. and Tolar, P. (2018) 'Mechanics of antigen extraction in the B cell synapse', *Mol*
880 *Immunol*, 101, 319-328, available: http://dx.doi.org/10.1016/j.molimm.2018.07.018.

881 Suzuki, K., Grigorova, I., Phan, T.G., Kelly, L.M. and Cyster, J.G. (2009) 'Visualizing B cell
882 capture of cognate antigen from follicular dendritic cells', *J Exp Med*, 206(7), 1485-93, available:
883 http://dx.doi.org/jem.20090209 [pii]10.1084/jem.20090209.

884 Tam, C., Idone, V., Devlin, C., Fernandes, M.C., Flannery, A., He, X., Schuchman, E., Tabas, I.
885 and Andrews, N.W. (2010) 'Exocytosis of acid sphingomyelinase by wounded cells promotes

endocytosis and plasma membrane repair', *J Cell Biol*, 189(6), 1027-38, available: http://dx.doi.org/jcb.201003053 [pii]10.1083/jcb.201003053.

Tanaka, S. and Baba, Y. (2020) 'B Cell Receptor Signaling', *Adv Exp Med Biol*, 1254, 23-36, available: http://dx.doi.org/10.1007/978-981-15-3532-1_2.

Tay, B., Stewart, T.A., Davis, F.M., Deuis, J.R. and Vetter, I. (2019) 'Development of a high-throughput fluorescent no-wash sodium influx assay', *PLoS One*, 14(3), e0213751, available: http://dx.doi.org/10.1371/journal.pone.0213751.

Vidard, L., Kovacsovics-Bankowski, M., Kraeft, S.K., Chen, L.B., Benacerraf, B. and Rock, K.L. (1996) 'Analysis of MHC class II presentation of particulate antigens of B lymphocytes', *J Immunol*, 156(8), 2809-18.

Villeneuve, J., Bassaganyas, L., Lepreux, S., Chiritoiu, M., Costet, P., Ripoche, J., Malhotra, V. and Schekman, R. (2018) 'Unconventional secretion of FABP4 by endosomes and secretory lysosomes', *J Cell Biol*, 217(2), 649-665, available: http://dx.doi.org/10.1083/jcb.201705047.

Wang, J., Lin, F., Wan, Z., Sun, X., Lu, Y., Huang, J., Wang, F., Zeng, Y., Chen, Y.H., Shi, Y., Zheng, W., Li, Z., Xiong, C. and Liu, W. (2018) 'Profiling the origin, dynamics, and function of traction force in B cell activation', *Sci Signal*, 11(542), available: http://dx.doi.org/10.1126/scisignal.aai9192.

Wang, J.C., Bolger-Munro, M. and Gold, M.R. (2018) 'Imaging the Interactions Between B Cells and Antigen-Presenting Cells', *Methods Mol Biol*, 1707, 131-161, available: http://dx.doi.org/10.1007/978-1-4939-7474-0_10.

906 Yuseff, M.I., Reversat, A., Lankar, D., Diaz, J., Fanget, I., Pierobon, P., Randrian, V.,
907 Larochette, N., Vascotto, F., Desdouets, C., Jauffred, B., Bellaiche, Y., Gasman, S., Darchen, F.,
908 Desnos, C. and Lennon-Dumenil, A.M. (2011) 'Polarized secretion of lysosomes at the B cell
909 synapse couples antigen extraction to processing and presentation', *Immunity*, 35(3), 361-74,
910 available: http://dx.doi.org/S1074-7613(11)00276-7 [pii]10.1016/j.immuni.2011.07.008.

911 Zhang, Z., Chen, G., Zhou, W., Song, A., Xu, T., Luo, Q., Wang, W., Gu, X.S. and Duan, S.
912 (2007) 'Regulated ATP release from astrocytes through lysosome exocytosis', *Nat Cell Biol*, 9(8),
913 945-53, available: http://dx.doi.org/10.1038/ncb1620.

914

915 **Figure legends**

916 **Figure 1. BCR binding to surface-associated ligands causes B-cell PM permeabilization.** (**A**)
917 Time-lapse images of a splenic B-cell incubated with αM-beads (1:2 cell:bead ratio) in the
918 presence of PI *(Video 1)*. (**B**) Percentages of B-cells bound to beads. (**C**) Percentages of PI-
919 positive (PI+) cells in bead-bound B-cells at 30 min. (**D**) Gate for bead-bound B-cells in forward
920 and side scatter flow cytometry dot plot. (**E**) Histograms of PI fluorescence intensity (FI) of αM-
921 and Tf-bead-bound B-cells after 30 min incubation, showing 1,000 cells per condition. (**F**)
922 Percentages of PI+ bead-bound B-cells after 30 min incubation with αM- or Tf-beads with or
923 without soluble αM (sαM). (**G**) Percentages of PI+ bead-bound B-cells after 30 min at indicated
924 cell:αM bead ratios. (**H**) Time-lapse images of a B-cell interacting with αM-PLB in the presence
925 of FM1-43 and PI (arrows, FM1-43 or PI entry, *Video 4*). (**I**) Mean fluorescence intensity of
926 FM1-43 (green lines) and PI (red lines) in a defined intracellular region of a permeabilized (top)
927 and non-permeabilized (bottom) cell over time. (**J**) Percentages of PI+ B-cells interacting with
928 αM- or Tf-PLB for 60 min. (**K**) Percentages of B-cells interacting with αM- or Tf-PLB for 30

929 min showing intracellular FM staining (FM+). Data points represent independent experiments
930 (mean ± SD) (B, C, F, G, J, K). Bars, 5 μm. *$p \leq 0.05$, **$p \leq 0.01$, ***$p \leq 0.005$, unpaired Student's
931 *t*-test (B, C, J, K) or one-way ANOVA (F).
932 **Figure supplement 1.** BCR binding to αM-beads causes localized PM permeabilization in B-
933 cells.
934 **Figure supplement 2.** Identification of bead-bound B-cells by flow cytometry.
935 **Figure supplement 3.** BCR binding to αM-beads does not increase apoptosis in B-cells.
936 **Figure supplement 4.** Sudden increases in intracellular staining with the lipophilic FM dye in B-
937 cells permeabilized by interaction with αM-PLB.
938 **Figure supplement 5.** The lipophilic FM dye enters B-cells permeabilized by αM-PLB and
939 stains the nuclear envelope.
940 **Figure supplement 6.** BCR cross-linking with soluble ligands does not permeabilize B-cells but
941 induces a punctate form of FM uptake at the cell periphery that is distinct from the massive FM
942 influx induced by surface-associated ligands.
943
944 **Figure 2. Extracellular Ponceau 4R quenches cytoplasmic CFSE in αM-PLB-permeabilized**
945 **B-cells. (A)** Flow cytometry histograms of CFSE FI in B-cells incubated with or without SLO
946 for 10 min in the presence or absence of Ponceau 4R, showing 8,500 cells per condition**. (B)**
947 Percentages of cells with reduced CFSE in the presence or absence of Ponceau 4R after
948 treatment with or without SLO. Data points represent independent experiments (mean ± SD). **(C)**
949 Time-lapse images of B-cells pre-stained with CFSE interacting with αM-PLB in the presence of
950 Ponceau 4R (arrows, cells with Ponceau 4R quenching of cytoplasmic CFSE) *(Video 5)*. **(D)**
951 Percentages of B-cells with more than 70% loss of CFSE FI after 60 min interaction with αM- or

Tf -PLB. Data points represent independent experiments (mean ± SD). **(E)** Timing of PI, FM1-43 entry or Ponceau 4R-mediated CFSE quenching in B-cells interacting with αM-PLB. Data points represent individual cells in at least four independent experiments (mean ± SD). **(F)** Cumulative percentages of total permeabilized B-cells detected over time in four independent experiments. Bars, 5 μm. $^{**}p \leq 0.01$, $^{***}p \leq 0.005$, unpaired Student's *t*-test (B, D) or one-way ANOVA (E).

Figure 3. BCR-mediated binding of HEL coupled to beads or expressed as a transmembrane protein on COS-7 cells causes B-cell PM permeabilization. (A) Flow cytometry histograms of PI FI in WT or MD4 B-cells incubated with αM- or HEL-beads for 30 min by flow cytometry, showing 1,000 cells per condition. (**B**) Percentages of WT and MD4 B-cells binding αM- or HEL-beads. Data points represent independent experiments (mean ± SD). (**C**) Percentages of PI+ bead-bound WT or MD4 B-cells after 30 min incubation. Data points represent independent experiments (mean ± SD). **(D)** Spinning disk time-lapse images of a MD4 B-cell (left panels) and a WT B-cell (right panels) interacting with a mHEL-GFP-expressing COS-7 cell in the presence of PI *(Videos 6 and 7)*. Arrows, clustering of mHEL-GFP during B-cell binding; arrowheads, PI entry in the B-cell. **(E)** Percentages of PI+ MD4 and WT B-cells interacting with COS-7 cells transfected with mHEL-GFP. **(F)** Percentages of PI+ MD4 B-cells interacting with COS-7 cells transfected with mHEL-GFP or mock-transfected. Data points (E and F) represent individual videos from 3~4 independent experiments (mean ± SD). Bars, 5 μm $^{*}p \leq 0.05$, $^{**}p \leq 0.01$, $^{***}p \leq 0.005$, unpaired Student's *t*-test (E, F) or one-way ANOVA (B, C).

Figure 4. PM permeabilization induced by surface-associated antigen depends on high-affinity BCR-antigen binding, BCR signaling, and non-muscle myosin II (NMII) motor activity. (**A**) Percentages of PI+ single bead-binding B-cells after incubation with HEL-, DEL-I- or Tf-beads (1:4 cell:bead ratio) for 30 min. Data points represent independent experiments (mean ± SD). (**B**) Mean fluorescence intensity (MFI) of phosphotyrosine (pY) in HEL-bead-bound B-cells treated or untreated (NT) with a Src kinase inhibitor (iSrc) by flow cytometry. Data points represent independent experiments (mean ± SD). (**C**) Western blot analysis of phosphorylated BTK (pBTK) and BTK in B-cells incubated with HEL-beads in the presence or absence of a BTK inhibitor (iBTK) for 30 min. (**D**) Percentages of PI+ HEL-bead-bound cells treated with iSrc or iBTK relative to not-treated (NT) at 30 min. Data points represent independent experiments (mean ± SD). (**E**) Spinning disk time-lapse images of BCR polarization (yellow arrow) in a B-cell incubated with αM-PLB in the presence of FM4-64 (white arrow, intracellular FM). (**F**) Timing of BCR polarization and FM entry of individual cells interacting with αM-PLB *(Video 8)*. Data points represent individual cells in three independent experiments (mean ± SD). (**G**) Confocal images of BCR and phosphorylated NMII light chain (pMLC) staining in B-cells interacting with αM- or Tf-beads (arrows, bead binding sites). (**H** and **I**) FI ratio (FIR) of BCR (**H**) and pMLC (**I**) staining at the bead-binding site relative to the opposite PM in αM- and Tf-bead-bound cells over time. Data represent the averages of three independent experiments (mean ± SD). (**J**) Percentages of PI+ bead-binding B-cells incubated with αM-beads for 30 min with or without blebbistatin (Bleb). Data points represent individual videos from three independent experiments (mean ± SD). (**K**) Percentages of bead-bound B-cells incubated with αM-beads for 30 min in the presence or absence of Bleb. Data points represent independent

996 experiments (mean ± SD). Bars, 5 μm. *$p \leq 0.05$, **$p \leq 0.01$, ***$p \leq 0.005$, ****$p \leq 0.001$, unpaired
997 Student's *t*-test (B, H, I, K) or one-way ANOVA (A, D, J).
998 **Figure supplement 1.** Impact of BCR-antigen affinity on B-cell-bead binding.
999 **Figure supplement 2.** B-cell binding to αM-PLB but not to Tf-PLB triggers BCR polarization
1000 first and PM permeabilization later.
1001 **Figure supplement 3.** BCR and phosphorylated myosin light chain (pMLC) polarize towards
1002 αM-bead binding sites.
1003
1004 **Figure 5. Antigen-induced permeabilization triggers lysosomal exocytosis.** (**A**) Flow
1005 cytometry analysis of surface-exposed (no detergent permeabilization) and/or intracellular
1006 LIMP-2 (with detergent permeabilization) of bead-bound B-cells after incubation with αM- or
1007 Tf-beads for 30 min, showing 3,000 cells per condition. (**B** and **C**) Percentages of cells with
1008 surface-exposed LIMP-2 (relative to values with secondary antibody alone) in bead-bound B-
1009 cells incubated with αM- or Tf-beads (**B**) or with HEL-, DEL-I- or Tf-beads (**C**) for 30 min. Data
1010 points represent independent experiments (mean ± SD). (**D**) Confocal images of surface-exposed
1011 LIMP-2 in B-cells incubated with αM- or Tf-beads (arrows, bead-binding sites). (**E**) FIR (bead-
1012 binding site:opposite PM) of surface-exposed LIMP-2 in individual cells over time. Data points
1013 represent individual cells (mean ± SD). (**F**) Total internal reflection microscopy (TIRF) images
1014 (left) and FI surface plots (right) of SiR-Lyso at the B-cell surface contacting αM-PLB (*Video*
1015 *10*). (**G**) Representative MFI versus time plot of a SiR-Lyso-loaded lysosome undergoing
1016 exocytosis. (**H**) SiR-Lyso exocytosis events (circles) in individual B-cells during the first 0-15
1017 min or 25–45 min of incubation with αM-PLB. (**I**) Timing of individual SiR-Lyso exocytosis
1018 events in B-cells incubated with αM-PLB for 45 min. Data points represent individual SiR-Lyso

exocytosis events from three independent experiments (mean ± SD). (**J**) Numbers of SiR-Lyso exocytosis events per B-cell permeabilized (PI+) or not permeabilized (PI-) by αM-PLB during 45 min. Data points represent individual cells from three independent experiments (mean ± SD). *$p \leq 0.05$, **$p \leq 0.01$, unpaired Student's *t*-test (B and J) or one-way ANOVA (C and E). Bars, 5 μm.

Figure supplement 1. BCR-mediated binding of αM-beads induces surface exposure of the LIMP-2 luminal domain at bead contact sites.

Figure supplement 2. Detection of lysosomal exocytosis by TIRF microscopy.

Figure 6. Antigen-permeabilized B-cells reseal their PM in a lysosomal exocytosis-dependent manner. (**A**) B-cells were incubated with αM-beads and permeabilized/resealed cells were assessed by flow cytometry of FM4-64 (added from the start) and SYTOX Blue (added in the last 10 min) FI, in the presence or absence of BEL. (**B**) Percentages of permeabilized αM-bead-bound cells that resealed in the presence or absence of BEL. Data points represent independent experiments (mean ± SD). **(C)** Time-lapse images of splenic B-cells incubated with αM-PLB in the presence of SYTOX Green. PI was added for 10 min at the end *(Video 11)*. Arrows, cells that became permeabilized after contacting the αM-PLB and later excluded PI; arrowhead, cell that was SYTOX+ since the start of the video and did not exclude PI. *$p \leq 0.05$, unpaired Student's *t*-test (B). Bar, 5 μm.

Figure supplement 1. BEL does not affect PM integrity and viability of B-cells.

Figure supplement 2. B-cell morphological changes occurring during permeabilization by surface-associated antigen are reversible.

Figure 7. Antigen-induced PM permeabilization promotes antigen internalization and presentation. (**A**) Confocal live imaging of a B-cell interacting with fluorescent αM-beads (arrows, internalized αM). (**B**) Percentages of cells containing internalized αM or Tf, bound or not to αM- or Tf-beads, over time. Data points represent individual fields in three independent experiments (mean ± SD). (**C**) Percentages of bead-bound B-cells with internalized αM in the presence or absence of Bleb after 60 min. Data points represent individual fields in four independent experiments (mean ±SD). (**D**) Confocal images (xz) of αM internalization in B-cells permeabilized (FM-high) or not permeabilized (FM-low) by αM-PLB after 60 min. (**E**) Percentages of B-cells, permeabilized (FM-high) or not permeabilized (FM-low) by αM-PLB, containing internalized αM over time. Data points represent individual fields in three independent experiments (mean ± SD). (**F**) MFI values of internalized αM in individual B-cells permeabilized (FM-high) or not (FM-low) by αM-PLB over time. Data points represent independent experiments (mean ± SD). (**G**) IL-2 secretion by 3A9 T-cells activated by B-cells incubated with or without (no Ag) soluble HEL or DEL-I (10 µg/ml) for 72 h. Data points represent independent experiments (mean ± SD). (**H**) IL-2 secretion by 3A9 T-cells activated by B-cells incubated with or without HEL-, DEL-I- or Tf-beads (1:4 cell:bead ratio) for 72 h. Bars, 5 µm. Data points represent independent experiments (mean ± SD). *$p \leq 0.05$, **$p \leq 0.01$, **$p \leq 0.005$, ****$p \leq 0.0001$, unpaired Student's *t*-test (C,E,F), one-way ANOVA (G,H) or Kruskal-Wallis non-parametric test (B). (**I**) Cartoon depicting a working model for the spatiotemporal relationship of events initiated by the interaction of the BCR with surface-associated antigen. High-affinity binding stabilizes BCR-antigen interaction and induces strong BCR signaling (1) and NMII activation (2). Activated NMII generates local traction forces that permeabilize the PM (3), triggering a localized PM repair response mediated by lysosomal

exocytosis. Lysosome exocytosis releases hydrolases that cleave antigen off surfaces (4), facilitating endocytosis (5) and presentation to T-cells (6).

Supplementary materials for this manuscript include the following:

13 figure supplements

13 videos

Figure 1-figure supplement 1. BCR binding to αM-beads causes localized PM permeabilization in B-cells. (**A**) Live spinning-disk microscopy images of splenic B-cells incubated with αM- or Tf-beads before and after 60 min at 37°C in the presence of PI. The arrows point to bead-bound B-cells that became PI+ during the incubation (*Video 1*). (**B**) Live spinning disk time-lapse images and corresponding fluorescence intensity (FI) pseudo-color images of A20 B-cells incubated with αM-beads in the presence of PI. The arrow points to beads that caused permeabilization; the arrowhead points to the site of PI entry (*Video 2*). Beads appear faintly red due to autofluorescence. (**C**) Live spinning disk time-lapse images of splenic B-cells incubated with αM-beads in the presence of PI. The arrow points to a bead that was exchanged between cells (#1, #2) and caused permeabilization of cell #2 (*Video 3*). Bars, 5 μm

Figure 1-figure supplement 2. Identification of bead-bound B-cells by flow cytometry. Splenic B-cells were incubated with αM-conjugated yellow-green fluorescence beads in the presence of PI and analyzed by flow cytometry. Representative dot plots of side scatter (SSC) versus forward scatter (FSC) and fluorescence intensity histograms of yellow-green beads and PI are shown. Bead-bound B-cells were identified by sizes and the presence of yellow-green fluorescence.

Figure 1-figure supplement 3. BCR binding to αM-beads does not increase apoptosis in B-cells. Splenic B-cells treated or not with staurosporine for 24 h were incubated with αM- or Tf-beads for 30 min at 37°C, fixed, permeabilized, stained with antibodies against cleaved caspase-3, and analyzed by flow cytometry. (**A**) Identification of bead-bound and unbound B-cell populations on a side scatter (SSC) versus forward scatter (FSC) plot. The percentage of cells

positive for cleaved caspase-3 was determined in the bead-bound (**B**) or unbound (**C**) cell populations and expressed relative to the Tf-bead control. Data points represent independent experiments (mean ± SD). *$p \leq 0.05$; ***$p \leq 0.005$, unpaired Student's *t*-test.

Figure 1-figure supplement 4. Sudden increases in intracellular staining with the lipophilic FM dye in B-cells permeabilized by interaction with αM-PLB. (A) Live spinning disk time-lapse images of splenic B-cells (permeabilized or non-permeabilized) after contact with αM-PLB in the presence of FM1-43 and PI at 37°C. The arrows point to B-cell sites where intracellular FM or PI was initially detected. (B) Mean fluorescence intensity (MFI) of FM (green) and PI (red) over time in a defined intracellular region (*Video 4*) in permeabilized (left, 5 examples) or non-permeabilized cells (right, 5 examples). Bar, 5 μm.

Figure 1-figure supplement 5. The lipophilic FM dye enters B-cells permeabilized by αM-PLB and stains the nuclear envelope. The images show 8 examples of FM4-64 nuclear envelope staining (arrows) in splenic B-cells permeabilized by αM-PLB after 60 min incubation at 37°C and imaged by live spinning disk fluorescence microscopy. Bar, 5 μm.

Figure 1–figure supplement 6. BCR cross-linking with soluble ligands does not permeabilize B-cells but induces a punctate form of FM uptake at the cell periphery that is distinct from the massive FM influx induced by surface-associated ligands. Spinning disk time-lapse images of B-cells pre-labeled with soluble anti-BCR antibodies and FM1-43 (green) at 4°C and then imaged at 37°C after addition of secondary fluorochrome-labeled crosslinking antibodies (magenta), in the presence of FM1-43 (green) and PI (red, not detected). The arrows

point to areas at the cell periphery where small puncta of internalized FM1-43 were visualized next to anti-BCR clusters (*Video 4*). No PI influx was detected, indicating that the B-cells were not permeabilized. Bars, 5μm.

Figure 4-figure supplement 1. Impact of BCR-antigen affinity on B-cell-bead binding. Splenic B-cells were incubated with HEL, DEL-I or Tf-beads at the indicated cell:bead ratios for 30 min at 37^{o}C and analyzed by flow cytometry. (**A**) Representative SSC versus FSC dot plots gated for bead-bound populations. Outlined areas indicate populations of cells binding one single bead. (**B**) Percentages of total B-cells that bound to beads. Data points represent independent experiments (mean ± SD). (**C**) Percentages of bead-bound B-cells binding one single bead. Data points represent independent experiments (mean ± SD). No statistically significant differences were detected (one-way ANOVA).

Figure 4-figure supplement 2. B-cell binding to αM-PLB but not to Tf-PLB triggers BCR polarization first and PM permeabilization later. (**A**) Splenic B-cells stained for surface BCR (green) were incubated with Tf-PLB (top panels) or αM-PLB (bottom panels) for 60 min at 37^{o}C in the presence of FM4-64 (red) and imaged by live spinning disk fluorescence microscopy. (**B**) Percentages of B-cells with BCR polarization after incubation with Tf- or αM-PLB. Data points represent independent experiments (mean ± SD). ***$p \leq 0.005$, unpaired Student's *t*-test.

Figure 4-figure supplement 3. BCR and phosphorylated myosin light chain (pMLC) polarize towards αM-bead binding sites. The images show several examples of splenic B-cells stained for surface BCRs with a Cy3-labeled Fab fragment of donkey anti-mouse IgM+G (red),

incubated with αM (left, 5 examples)- or Tf (right, 5 examples)-beads, fixed, permeabilized, and stained for pMLC (magenta) and analyzed by confocal fluorescence microscopy. The arrows point to bead contact sites in B-cells. Bars, 3 μm.

Figure 5-figure supplement 1. BCR-mediated binding of αM-beads induces surface exposure of the LIMP-2 luminal domain at bead contact sites. The images show several examples of splenic B-cells incubated with αM (left)- or Tf (right)-beads for 30 min at 37^{o}C, stained with LIMP-2-specific antibodies (green) at 4^{o}C without detergent permeabilization, followed by fixation, staining with secondary antibodies, and analysis by confocal fluorescence microscopy. Arrows, sites of bead binding on B-cells. Bar, 5 μm.

Figure 5-figure supplement 2. Detection of lysosomal exocytosis by TIRF microscopy. Splenic B-cells were added to αM-PLB and imaged by TIRF at 8 frames/s. Live time-lapse XY images of individual SiR-Lyso puncta (top rows), their FI surface plots (bottom rows), and MFI (plots on right) within the TIRF evanescent field over time are shown for 4 examples where lysosomal exocytosis occurred (**A**, rapid decrease in MFI, consistent with rapid dye loss upon PM fusion) or not (**B**, slow reduction in MFI, likely due to lysosome movement away from the PM).

Figure 6-figure supplement 1. BEL does not affect the PM integrity and viability of B-cells. Splenic B-cells were pretreated or not with BEL and incubated with αM-beads in the presence of FM4-64 and analyzed by flow cytometry. (A) Representative dot plots of side scatter (SSC) versus forward scatter (FSC) of B-cells incubated with αM-beads. Outlined areas indicate the

low SSC/FSC populations that correspond to dead cells. (B) Percentage of low SSC/FSC B-cells incubated with αM-beads treated or not with BEL. Data points represent independent experiments (mean ± SD). (C) Representative dot plots of side scatter (SSC) versus forward scatter (FSC) of B-cells incubated with Tf-beads in the presence of SYTOX Blue throughout the experiment (30 min) or only in the last 5 min. Outlined areas indicate B-cell populations binding Tf beads. (D) Percentages of SYTOX Blue-positive (+). Tf-bead-bound cells. Data points represent independent experiments (mean ± SD). No statistically significant differences were detected (Student's *t*-test).

Figure 6 – figure supplement 2. B-cell morphological changes occurring during permeabilization by surface-associated antigen are reversible. Spinning disk time-lapse images of B-cells interacting with αM-PLB in the presence of PI (red). The dashed line indicates the maximum cell diameter initially reached by a B-cell that became permeabilized, allowing PI influx *(Video 12)*. The later frames indicate that the cell gradually recovers its original morphology. Bars, 5μm.

Video 1. BCR binding to αM-beads permeabilizes the PM of splenic B-cells. Splenic B-cells were incubated with αM-beads at 4°C and warmed to 37°C in a live imaging chamber with 5% CO_2 in DMEM-BSA. Time-lapse images were acquired for 60 min at 1 frame/15 s in the presence of PI (red) using a spinning disk fluorescence microscope (UltraVIEW VoX, PerkinElmer with a 63X 1.4 N.A. oil objective). The arrow indicates the moment of PI entry. Time is displayed as hour: minutes: seconds. The video is displayed at 20 frames/s. Bar, 5 μm.

Video 2. BCR binding to αM-beads causes localized PM permeabilization in A20 B-cells (cell line). A20 B-cells were incubated with αM-beads in a live imaging chamber at 37°C with 5% CO_2 in DMEM/BSA. Time-lapse images were acquired for 65 min at 1 frame/20 s in the presence of PI using a spinning disk fluorescence microscope (UltraVIEW VoX, PerkinElmer with a 63X 1.4 N.A. oil objective). The arrow points to the beads and the arrowhead points to the site of entry and subsequent flow of PI into the cell. Beads appear red as a result of autofluorescence. Time is displayed as hour: minutes: seconds. The video is displayed at 20 frames/s. Bar, 5 μm.

Video 3. Bead exchange between B-cells causes PM permeabilization. Splenic B-cells were incubated with αM-beads in a live imaging chamber at 37°C with 5% CO_2 in DMEM-BSA. Images were acquired for 60 min at 1 frame/30 s in the presence of PI using a spinning disk fluorescence microscope (UltraVIEW VoX, PerkinElmer with a 63X 1.4 N.A. oil objective). The arrow points to the bead that was exchanged between cells (#1 and #2) and caused permeabilization of cell #2. Beads appear red as a result of autofluorescence. Time is displayed as hour: minutes: seconds. The video is displayed at 10 frames/s. Bar, 5 μm.

Video 4 – Surface-associated ligand induces B-cell permeabilization and massive FM influx, while soluble ligand does not cause permeabilization but induces endocytosis, detected as puncta at the cell periphery. Top: B-cells pre-labeled with FM1-43 (green) were added to αM-PLB (surface-associated ligand). Bottom: B-cells pre-labeled with FM1-43 (green) and anti-BCR antibodies followed by secondary fluorochrome-labeled crosslinking antibodies (magenta)

(soluble ligand). Under both conditions cells were imaged at 37°C in the presence of FM1-43 (green), and PI (red) was added to detect PM permeabilization. Images were acquired for 60 min at 1 frame/30 s or 15 s using a spinning disk fluorescence microscope (UltraVIEW VoX, PerkinElmer with a 60X 1.4 N.A. oil objective). Time is displayed as minutes: seconds after cells contacted αM-PLB. The white box indicates the intracellular area used to measure FI levels of intracellular FM1-43 (see Figure 1I and Figure 1-figure supplement 4). The arrow indicates the massive influx of FM1-43 in cells permeabilized during contact with αM-PLB. The arrowheads indicate areas where peripheral FM1-43 puncta (likely endosomes) were observed next to clusters of crosslinked BCR (magenta). The video is displayed at 20 frames/s. Bar, 5 μm.

Video 5. B-cell PM permeabilization during binding to αM-PLB enables membrane-impermeable Ponceau 4R to quench cytoplasmic CSFE fluorescence. Splenic B cells pre-labeled with CFSE in the cytosol were added to αM-PLB in a live imaging chamber at 37^{o}C with 5% CO_2 in DMEM/BSA. Images were acquired for 60 min at 1 frame/10 s in the presence of Ponceau 4R using a spinning disk fluorescence microscope (UltraVIEW VoX, PerkinElmer with a 40X 1.4 N.A. oil objective). The arrow indicates CFSE-labeled B-cells that lost their cytosolic fluorescence as a result of PM permeabilization and Ponceau 4R influx. Time is displayed as hour: minutes: seconds. The video is displayed at 30 frames/s. Bar, 5 μm.

Video 6. Binding of MD4 B-cells to COS-7 cells expressing surface mHEL-GFP induces antigen clustering and PM permeabilization at interaction sites. MD4 splenic B-cells were incubated with mHEL-GFP-expressing COS-7 cells cultured on fibronectin-coated coverslips at 37^{o}C with 5% CO_2 in DMEM/BSA. Images were acquired for 120 min at 1 frame/20 s in the

presence of PI using a spinning disk fluorescence microscope (UltraVIEW VoX, PerkinElmer with a 40X 1.3 N.A. oil objective). Shown are representative videos of XY (top) and XZ (bottom) views showing clustering of mHEL-GFP (arrows) and the intracellular influx of PI (arrowheads) at cell interacting sites. Time is displayed as minutes: seconds after the cell contacted the mHEL-GFP expressing COS cell. The video is displayed at 15 frames/s. Bar, 5 μm.

Video 7. Binding of WT B-cells to COS-7 cells expressing surface mHEL-GFP does not induce antigen clustering and PM permeabilization at interaction sites. WT splenic B-cells were incubated with mHEL-GFP-expressing COS-7 cells cultured on fibronectin-coated coverslips at 37°C with 5% CO_2 in DMEM/BSA. Images were acquired for 120 min at 1 frame/20 s in the presence of PI using a spinning disk fluorescence microscope (UltraVIEW VoX, PerkinElmer with a 40X 1.3 N.A. oil objective). Shown are representative videos of XY (top) and XZ (bottom) views. Time is displayed as minutes: seconds after the cell contacted the mHEL-GFP expressing COS cell. The video is displayed at 15 frames/s. Bar, 5 μm.

Video 8. The BCR polarizes towards antigen-binding sites before PM permeabilization. Splenic B-cells stained with anti-BCR antibodies were added to αM-PLB and imaged in a live imaging chamber at 37°C with 5% CO_2 in DMEM/BSA. Images were acquired for 60 min at 1 frame/20 s in the presence of FM4-64 using a spinning disk fluorescence microscope (UltraVIEW VoX, PerkinElmer with a 60X 1.4 N.A. oil objective). Top: XZ view showing BCR (green) polarization towards the αM-PLB (white arrow). Bottom: XY view showing intracellular influx of FM4-64 (red, yellow arrow). Time is displayed as minutes: seconds after the cell

contacted the αM-PLB. The video is displayed at 15 frames/s. Bar, 5 μm.

Video 9. BCR and phosphorylated non-muscle myosin II (pMLC) polarize towards αM-bead-binding sites on a B-cell. Shown is a 3D representation of co-polarization of the BCR (red) and pMLC (green) towards the site of αM-bead (white) binding in a splenic B-cell. Z-stack images were acquired using a Zeiss LSM710 confocal fluorescence microscope (63X 1.4 N.A. oil objective) and the 3D reconstruction was generated using Volocity software (PerkinElmer). Bar, 3 μm.

Video 10. A lysosomal exocytosis event detected by total internal reflection fluorescence (TIRF) microscopy. Splenic B-cells preloaded with SiR-Lyso were incubated with αM-PLB in a coverslip chamber at 37°C with 5% CO_2 in DMEM/BSA for 30 min. Time-lapse images were acquired for 20 min at 8 frames/s using a TIRF microscope (NIKON Eclipse Ti-E TIRF, 63X 1.49NA oil objective). Top: TIRF images of a lysosome appearing in the TIRF evanescent field and then rapidly losing the SiR-Lyso signal due to fusion with the B-cell PM. Bottom: FI surface plot corresponding to the video on the top. Time is displayed in seconds. The video is displayed at 15 frames/s.

Video 11 – B-cells exclude a second membrane-impermeable tracer after antigen-dependent permeabilization. Splenic B-cells were added to αM-PLB and imaged in a live imaging chamber at 37°C with 5% CO2 in DMEM 2% of FBS in the presence of SYTOX Green (green). Images were acquired for 4 h at 1 frame/30 s using a spinning disk fluorescence microscope (UltraVIEW VoX, PerkinElmer with a 60X 1.4 N.A. oil objective). PI (red) was

added for 10 min at the end of the time-lapse image acquisition. The video is displayed as minutes: seconds after the cell contacted the αM-PLB. White arrows indicate cells that became permeabilized and later excluded PI. The yellow arrow indicates a cell that was stained by SYTOX Green since the beginning of the video and was not able to exclude PI. The video is displayed at 20 frames/s. Bar, 5 μm.

Video 12. B-cell morphological changes occurring during permeabilization by surface-associated antigen are reversible. Splenic B-cells were added to αM-PLB and imaged in a live imaging chamber at 37^{o}C with 5% CO2 in DMEM without phenol red containing 2% FBS in the presence of PI (red). Images were acquired for 4 h at 1 frame/30 s using a spinning disk fluorescence microscope (UltraVIEW VoX, PerkinElmer with a 60X 1.4 N.A. oil objective). Time is displayed as minutes: seconds after the cells first contacted the αM-PLB. The arrow points to a cell that became permeabilized. The dashed line indicates the maximum diameter of the B-cell after permeabilization. The video is displayed at 20 frames/s. Bar, 5 μm.

Video 13. B-cell with polarized surface BCRs and containing fluorescent αM extracted from beads. The surface BCRs of splenic B-cells were labeled with Cy3-Fab-donkey anti-mouse IgM+G at 4^{o}C. Labeled B-cells were incubated with AF488-αM-beads at 37^{o}C with 5% CO_2 for 60 min and then fixed. Images were acquired using a Zeiss LSM710 (63X 1.4 N.A. oil objective), and the 3D reconstruction was generated with Volocity software (PerkinElmer). The arrow points to internalized AF488-αM.

Figure 1

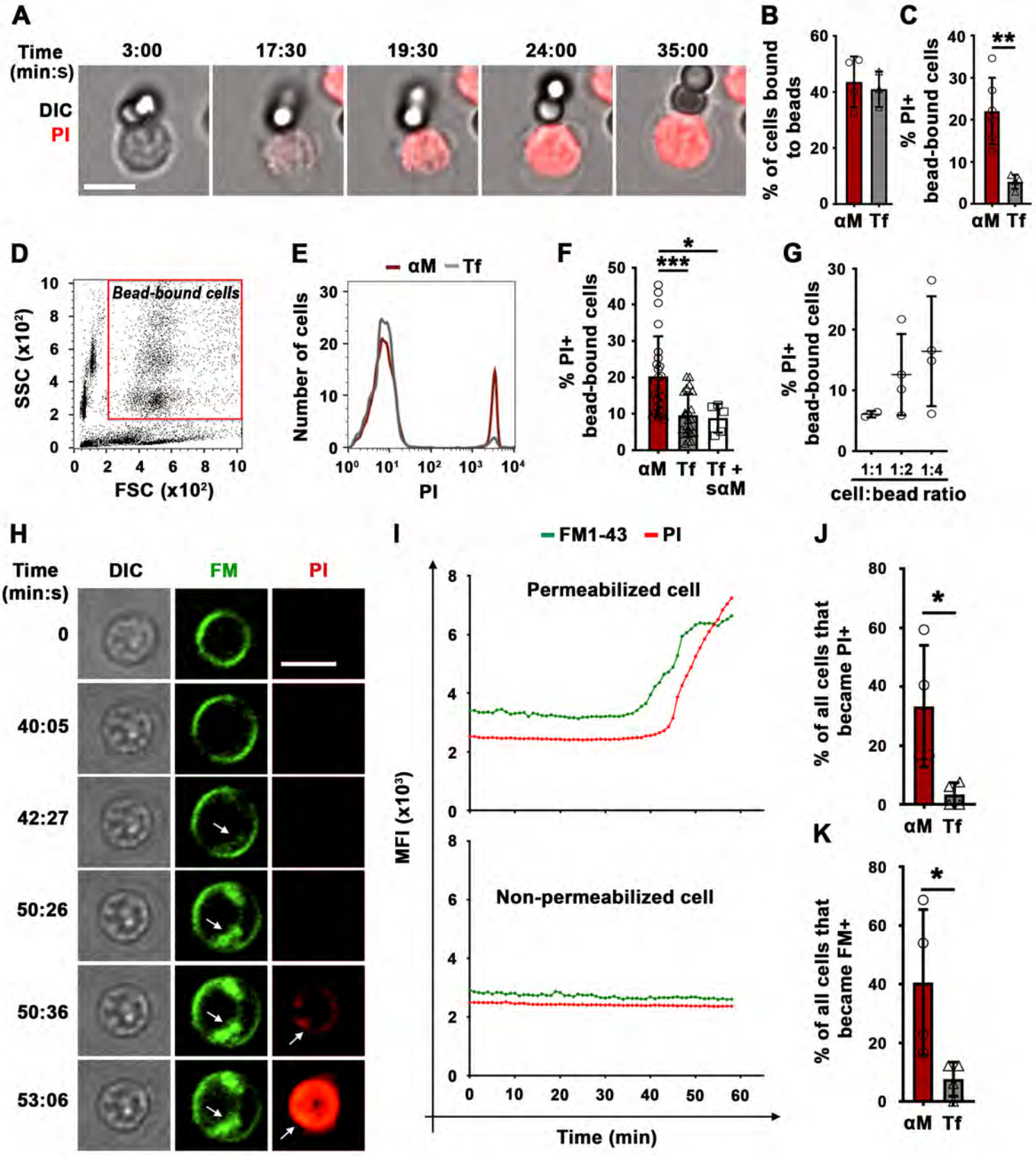

Figure 2

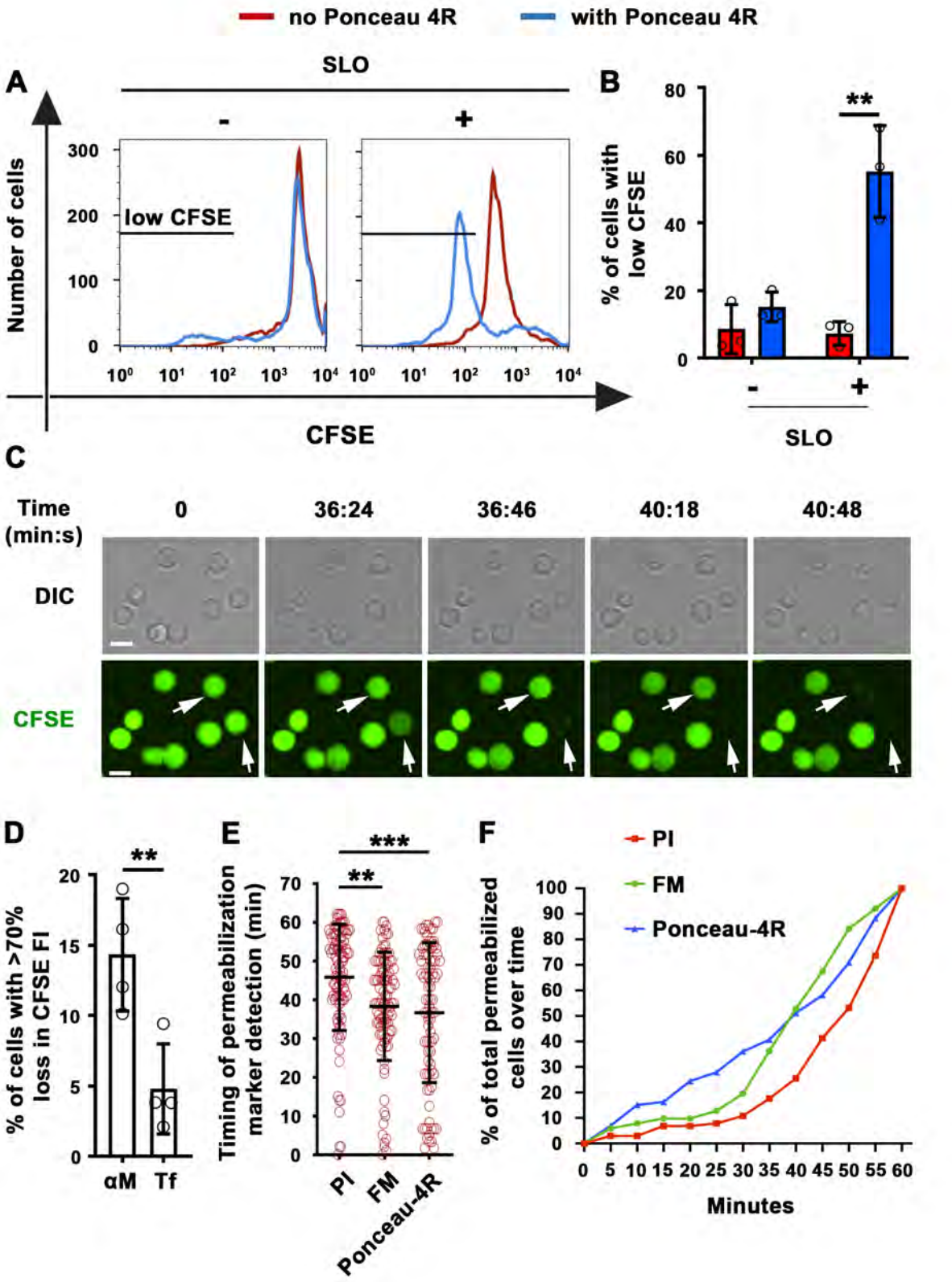

Figure 3

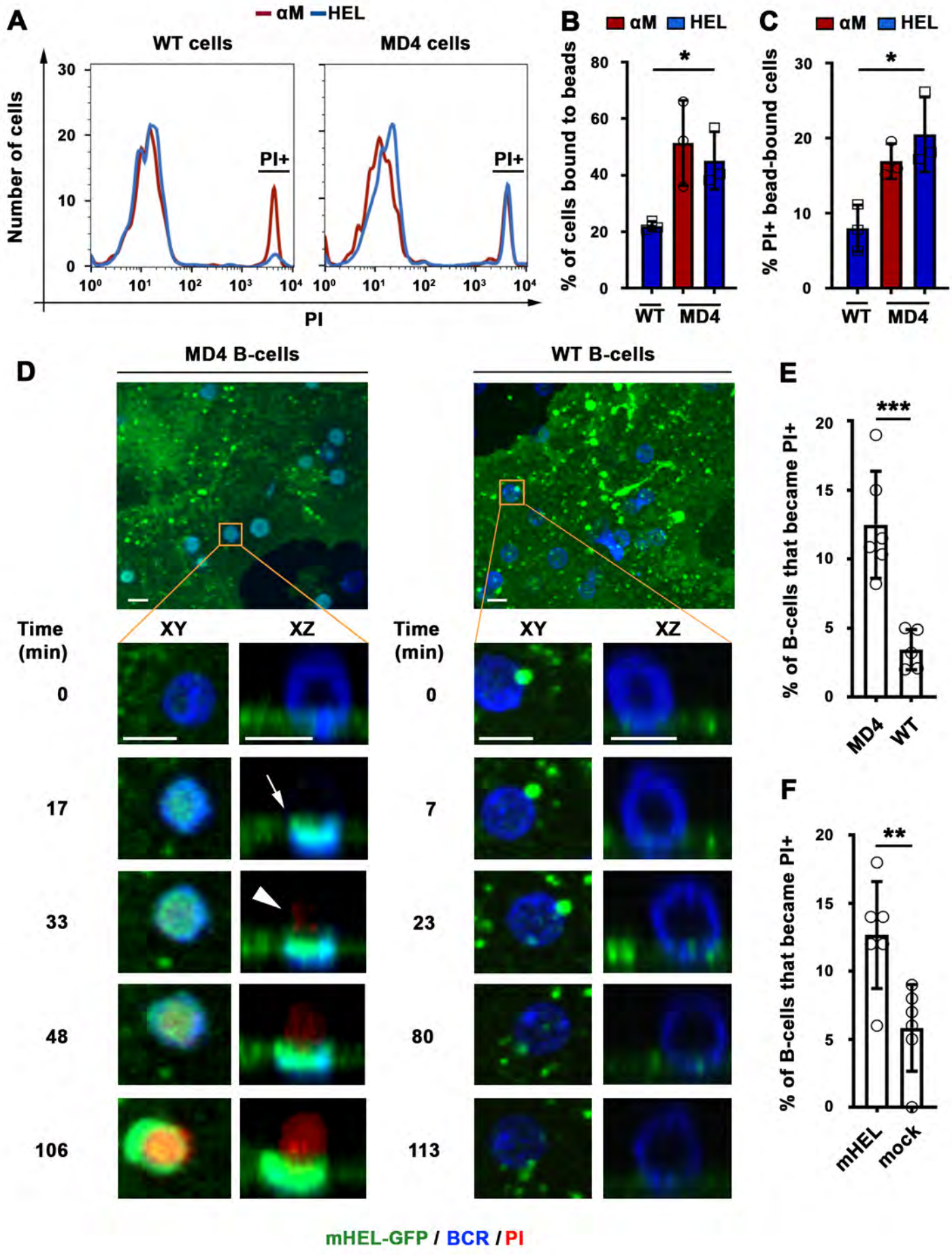

Figure 4

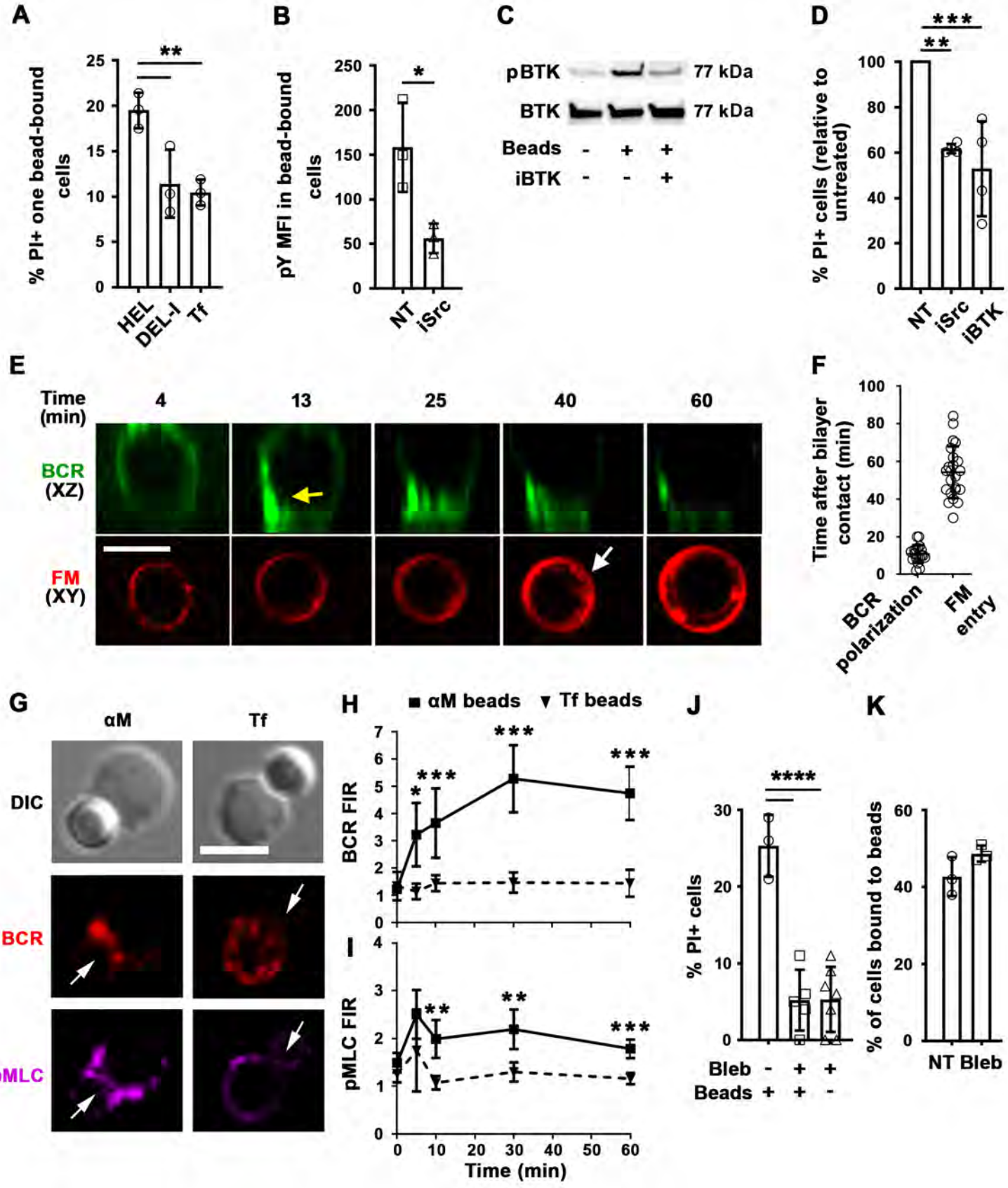

Figure 5

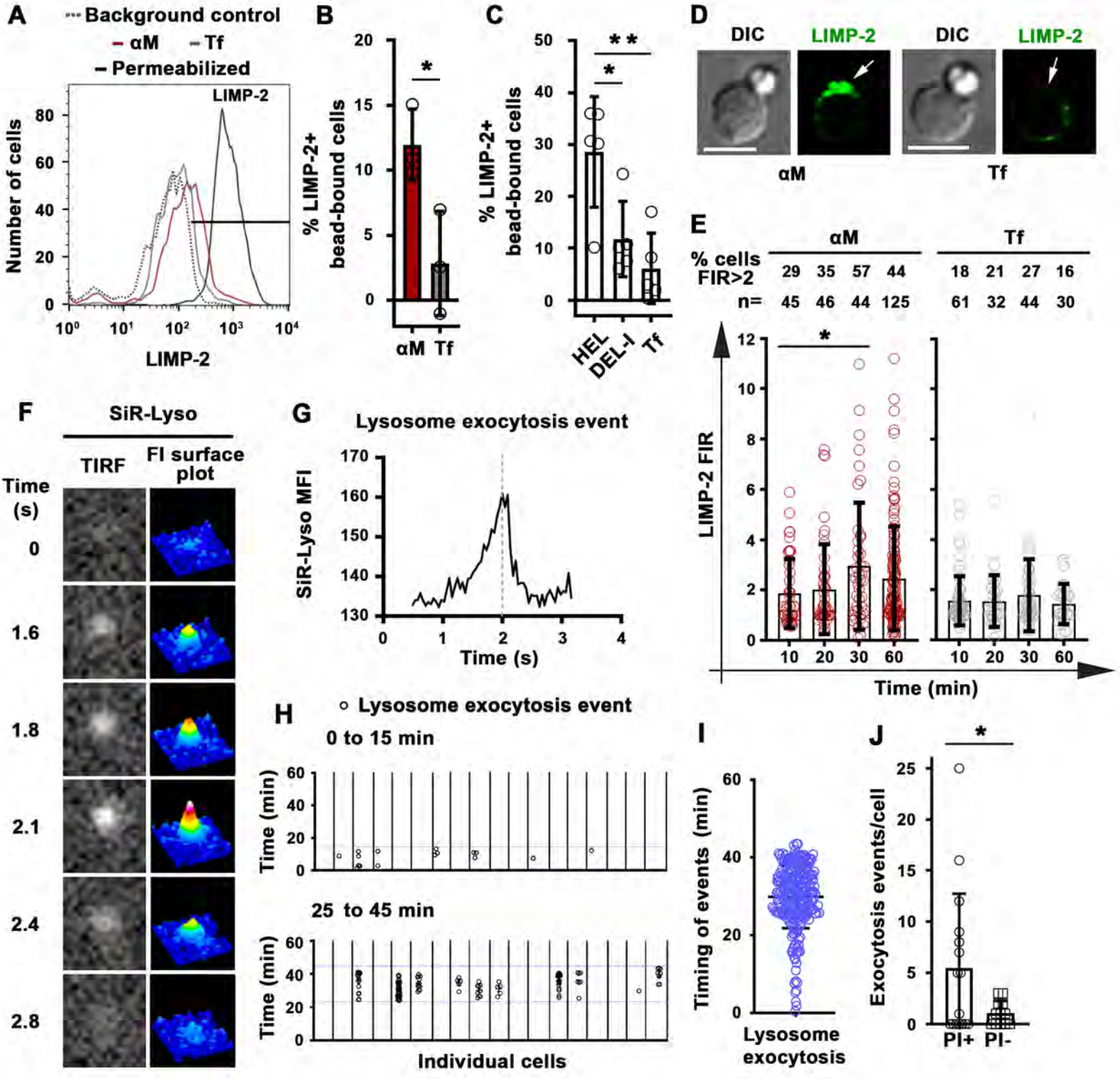

Figure 6

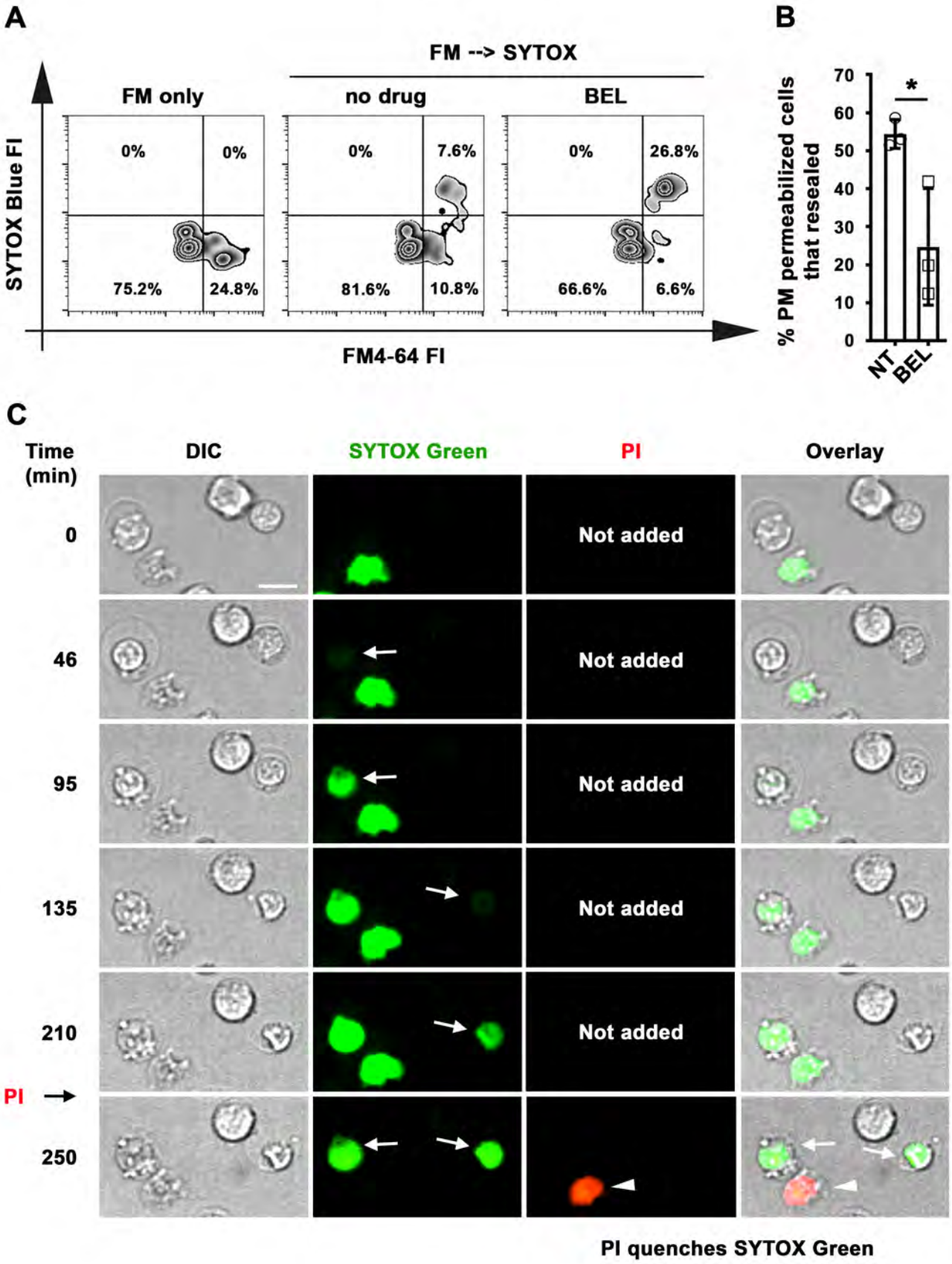

Figure 7

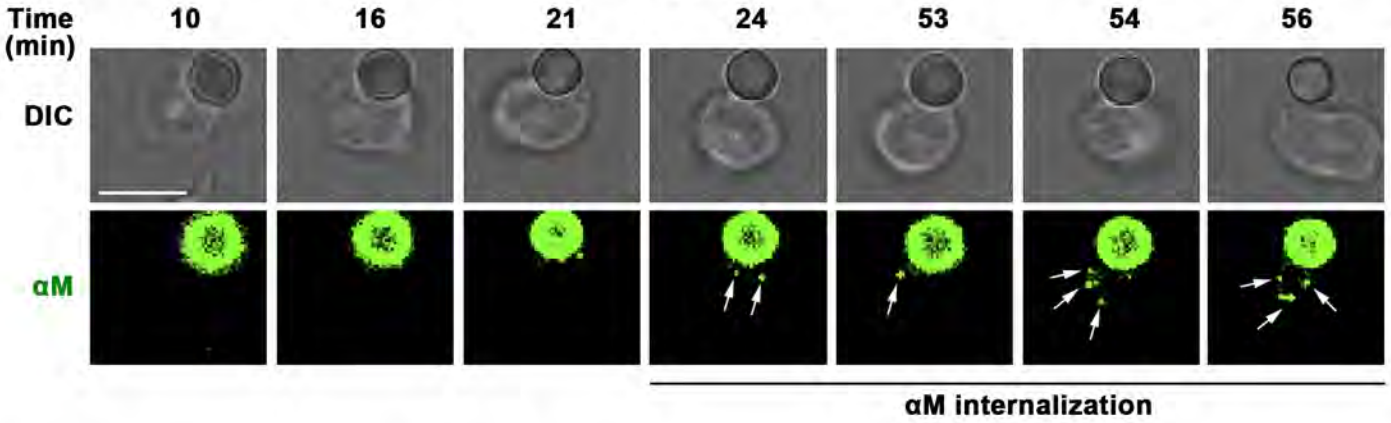

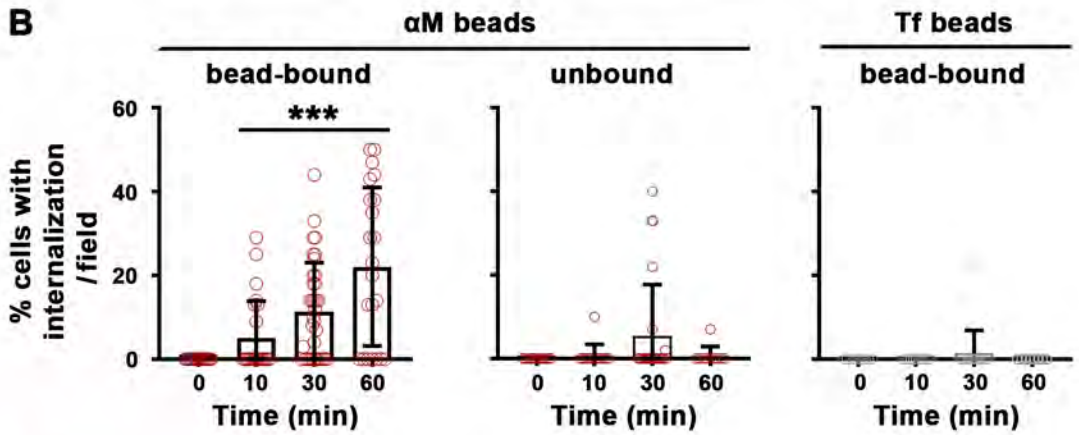

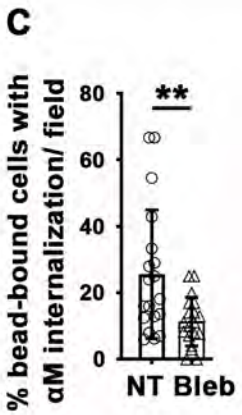

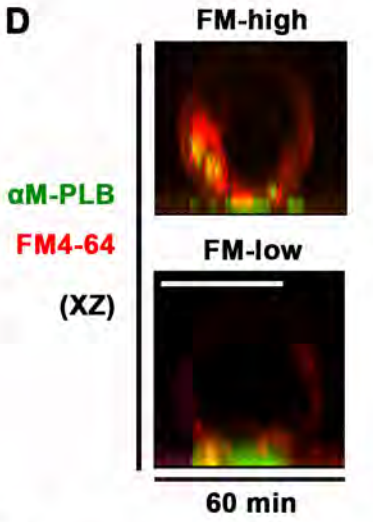

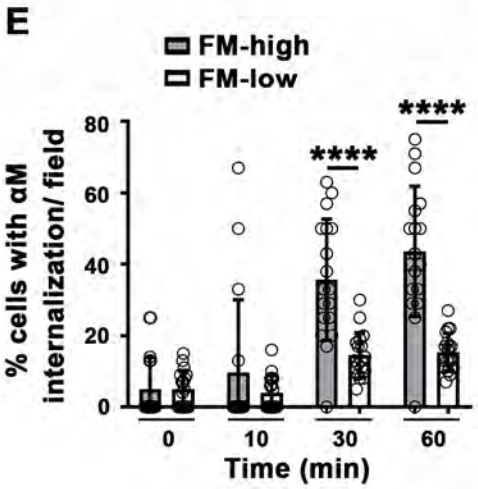

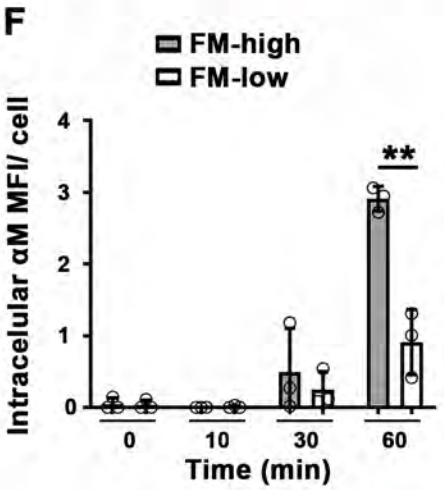

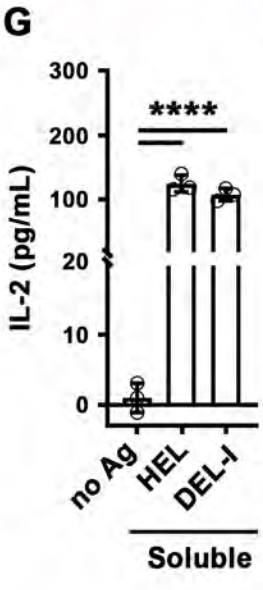

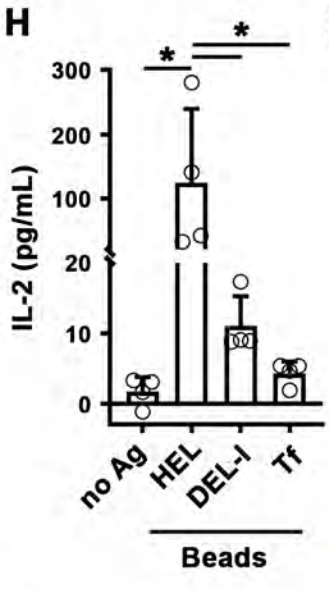

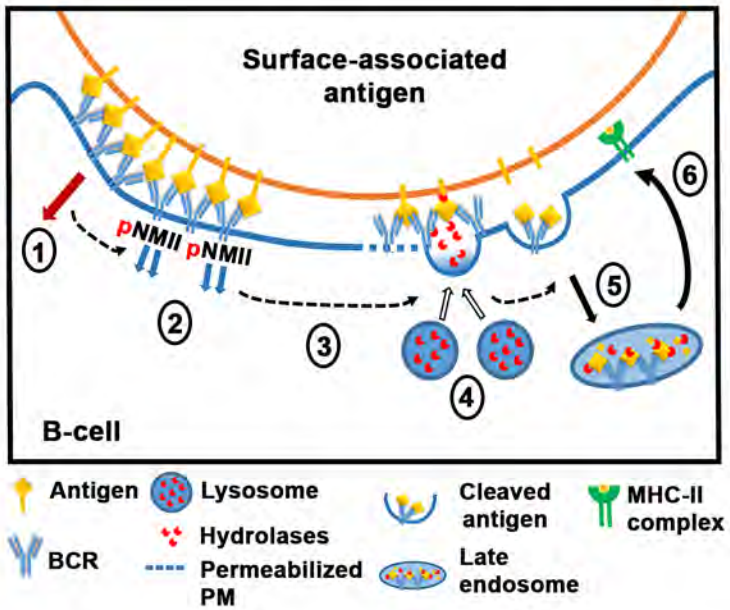

Figure 1- figure supplement 1

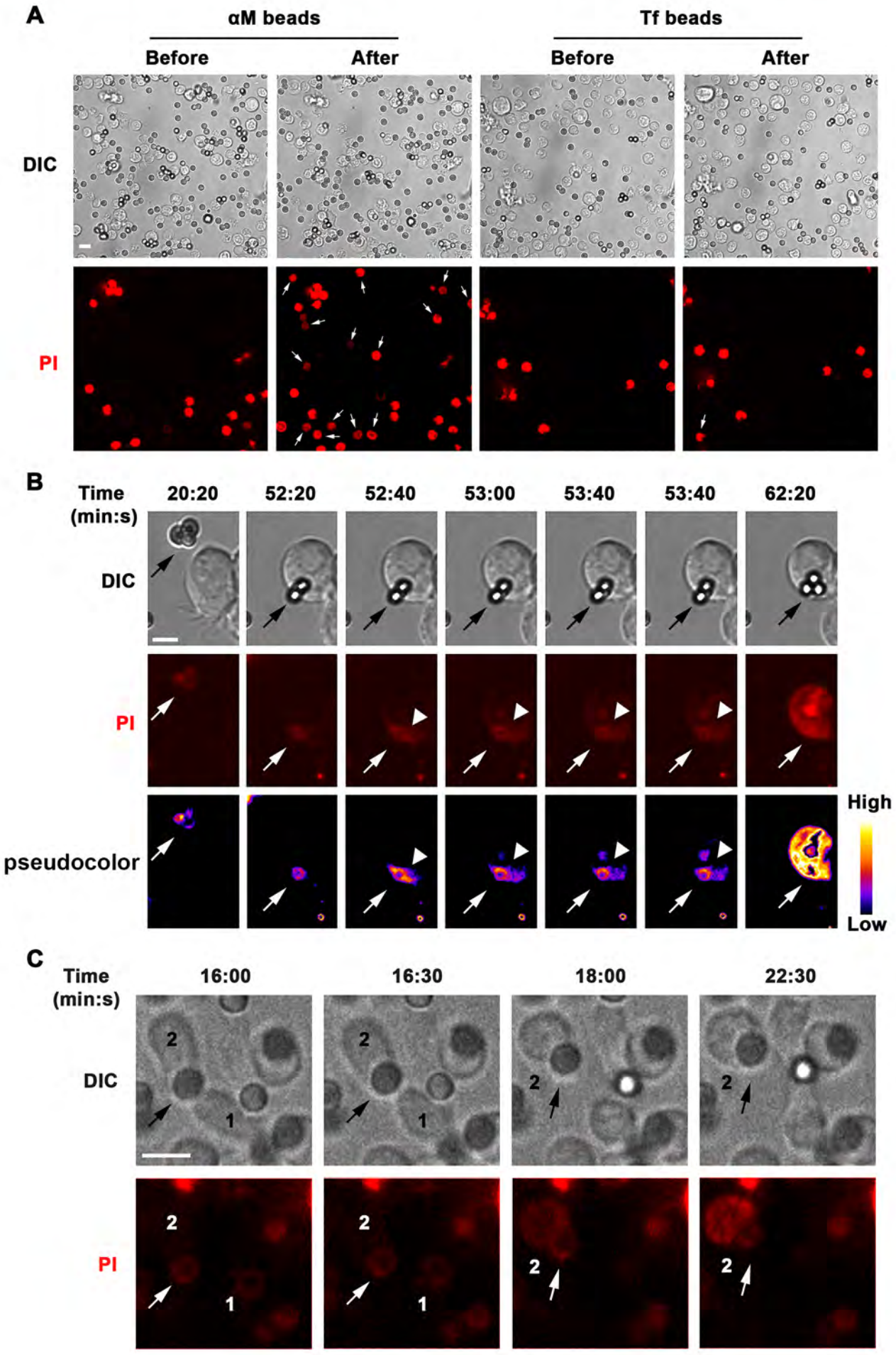

Figure 1- figure supplement 2

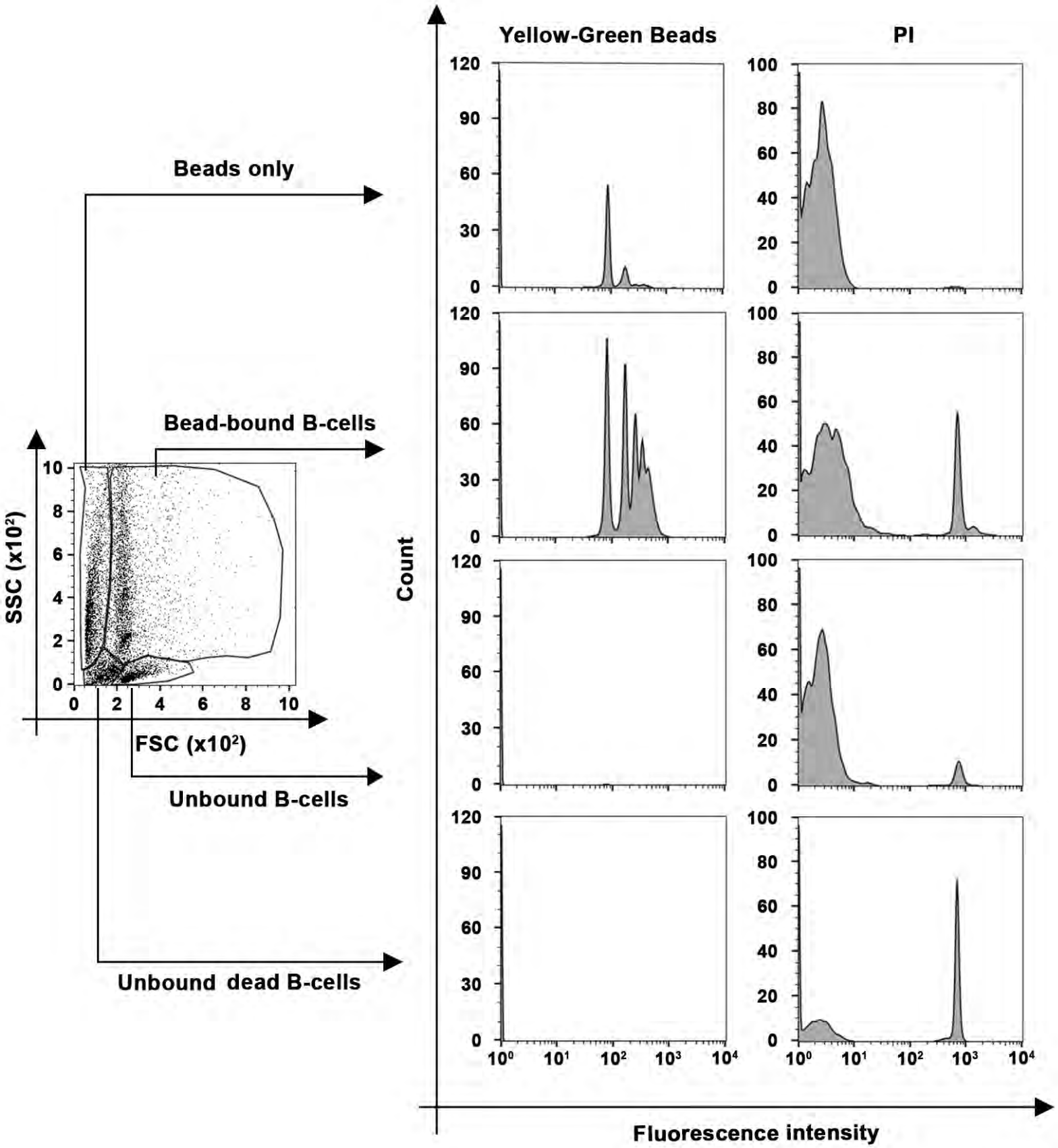

Figure 1- figure supplement 3

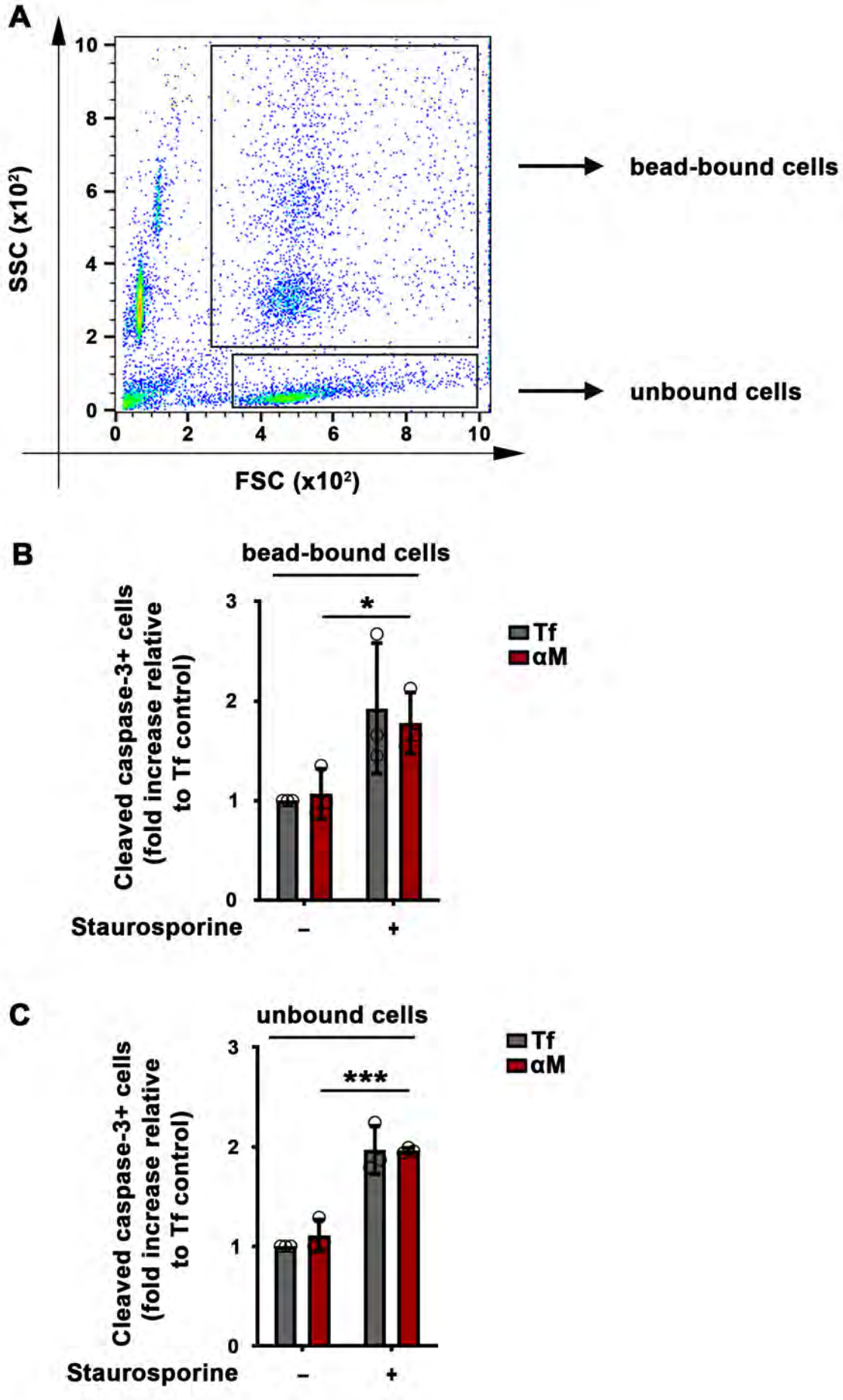

Figure 1- figure supplement 4

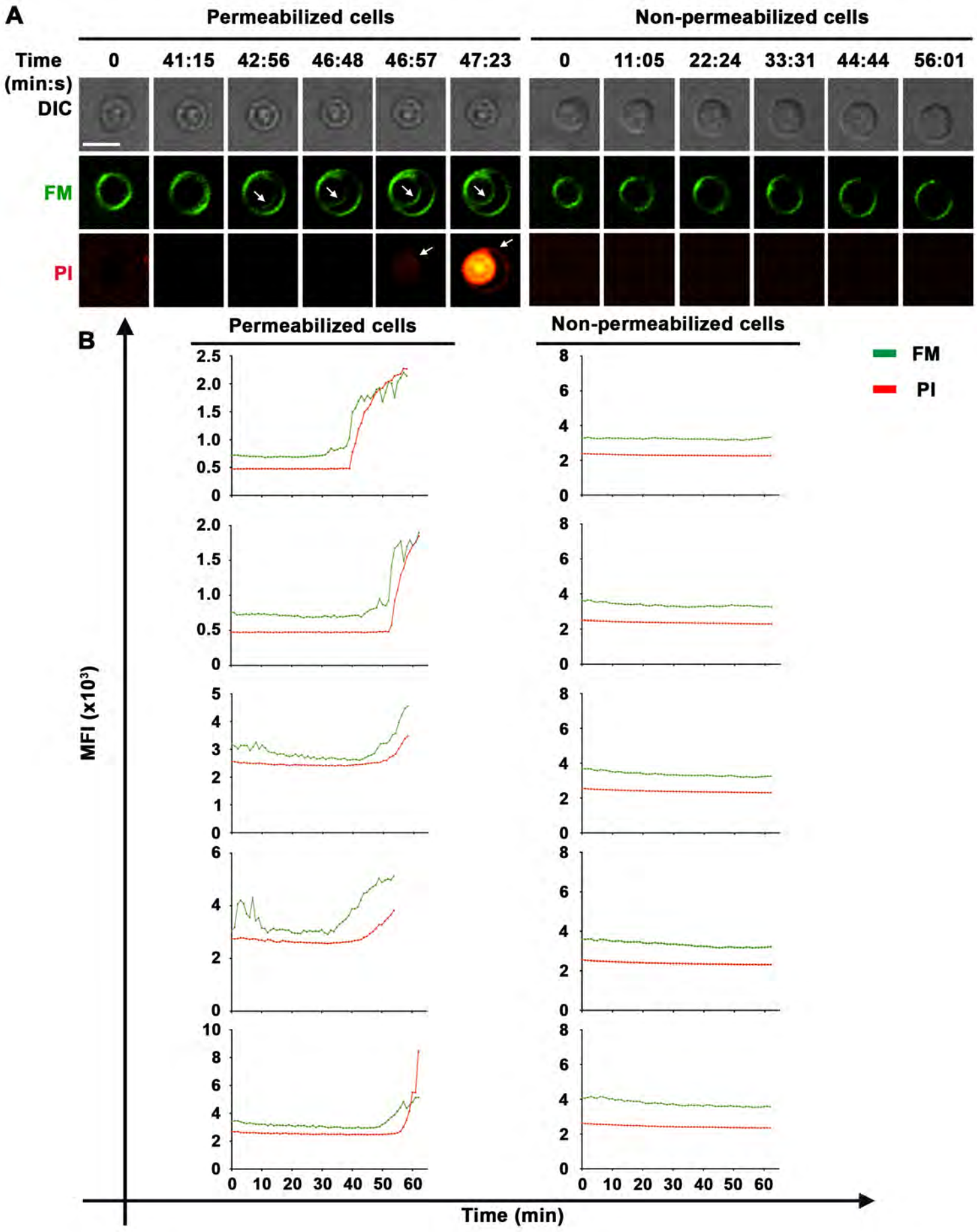

Figure 1- figure supplement 5

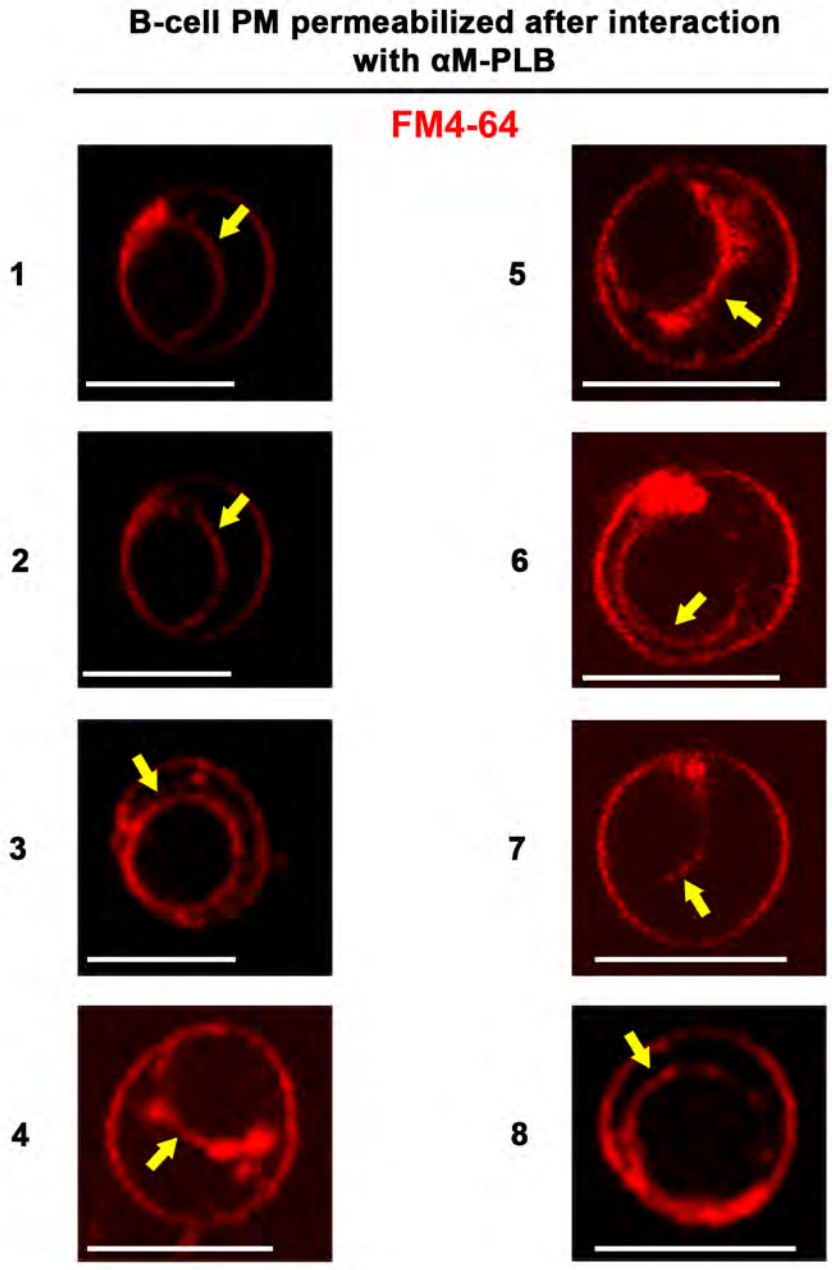

Figure 1- figure supplement 6

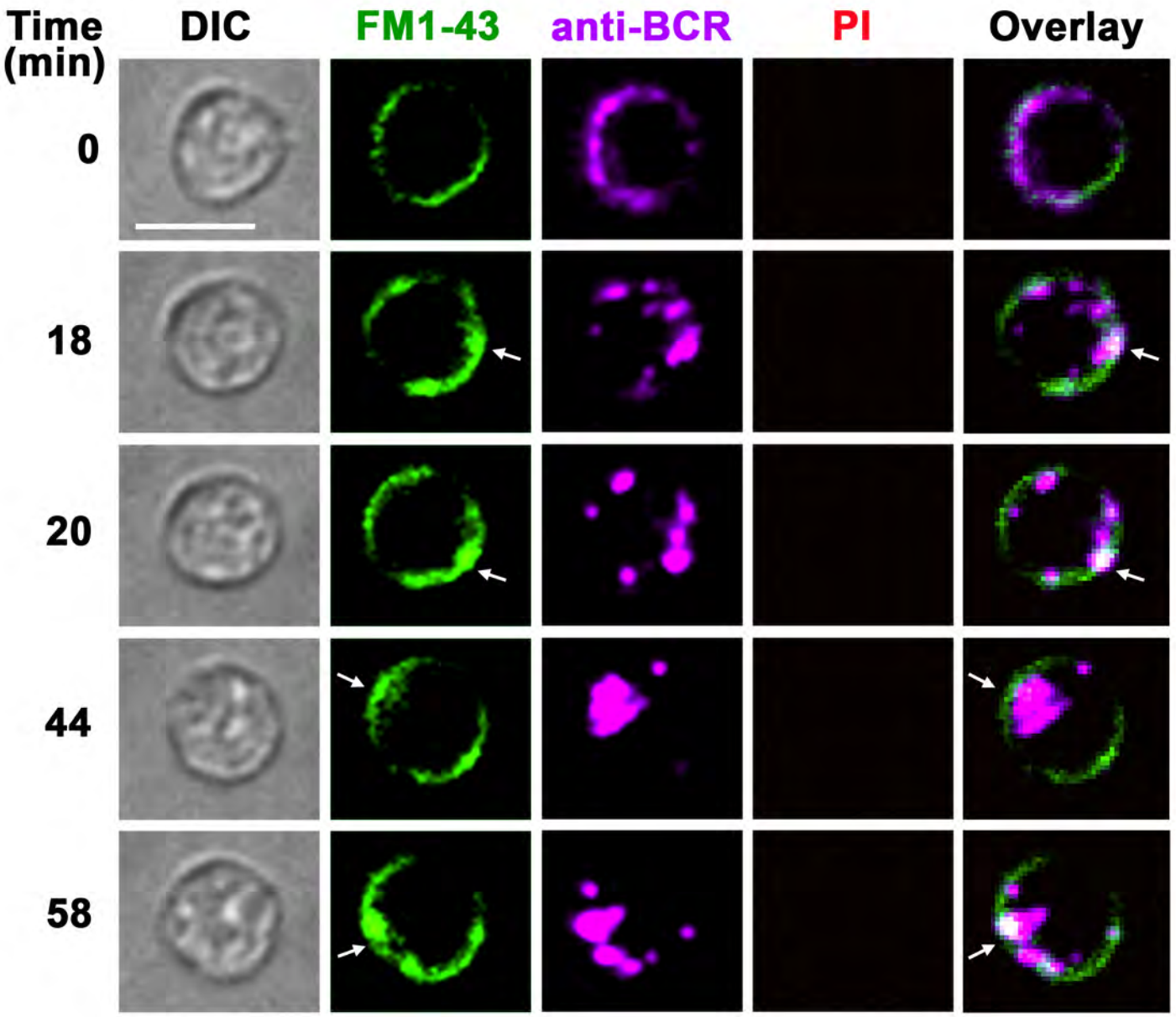

Figure 4- figure supplement 1

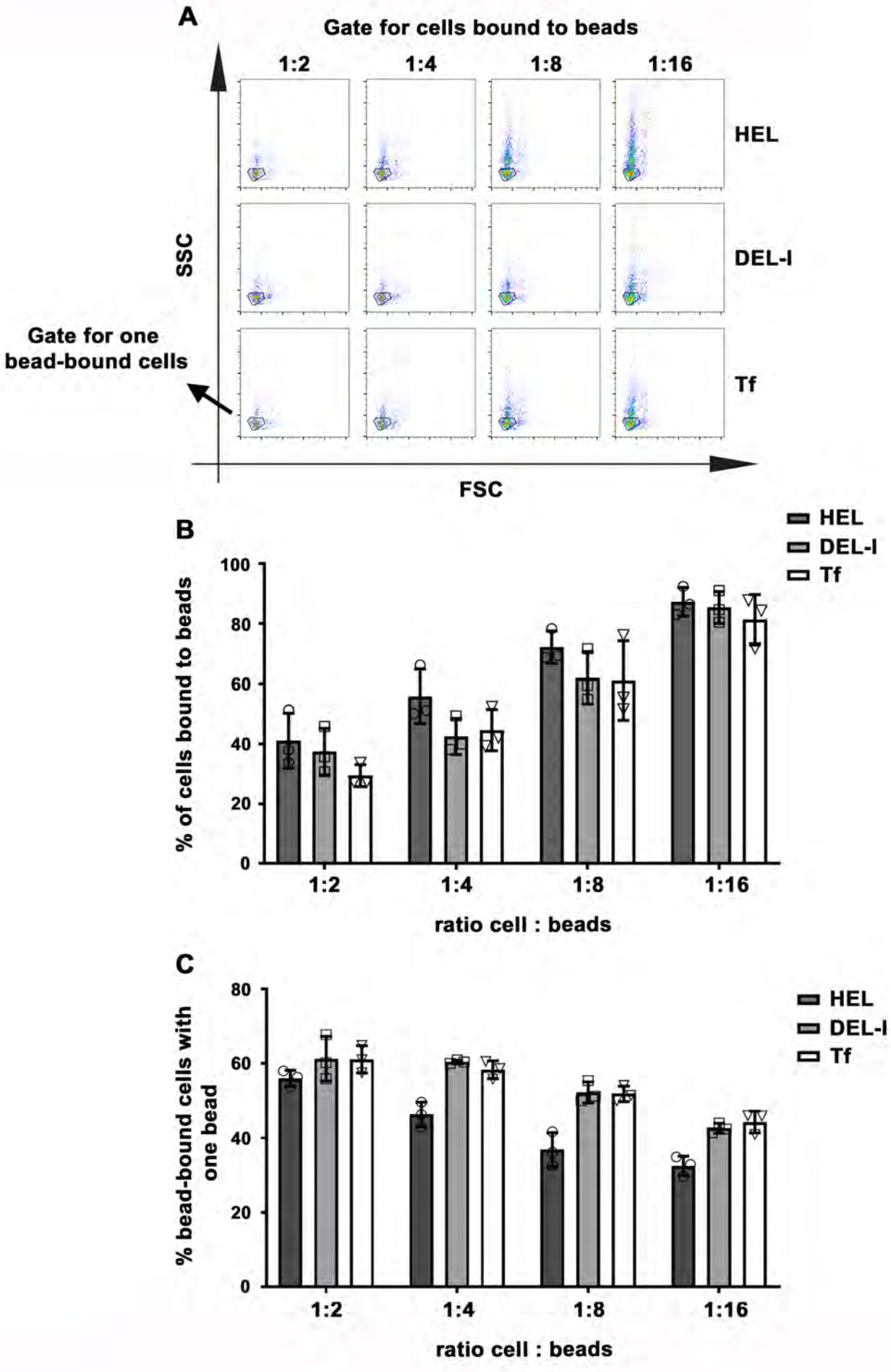

Figure 4- figure supplement 2

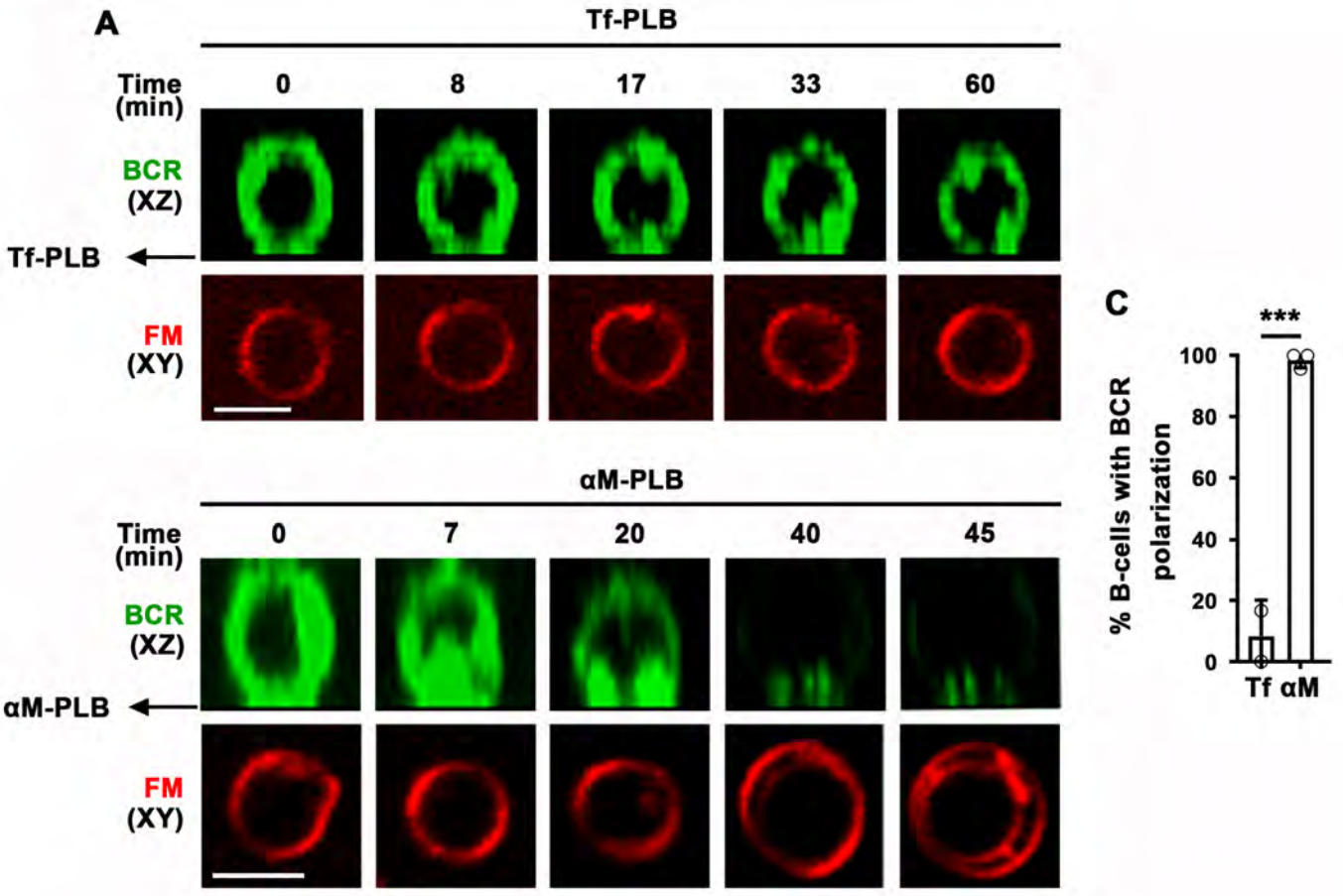

Figure 4- figure supplement 3

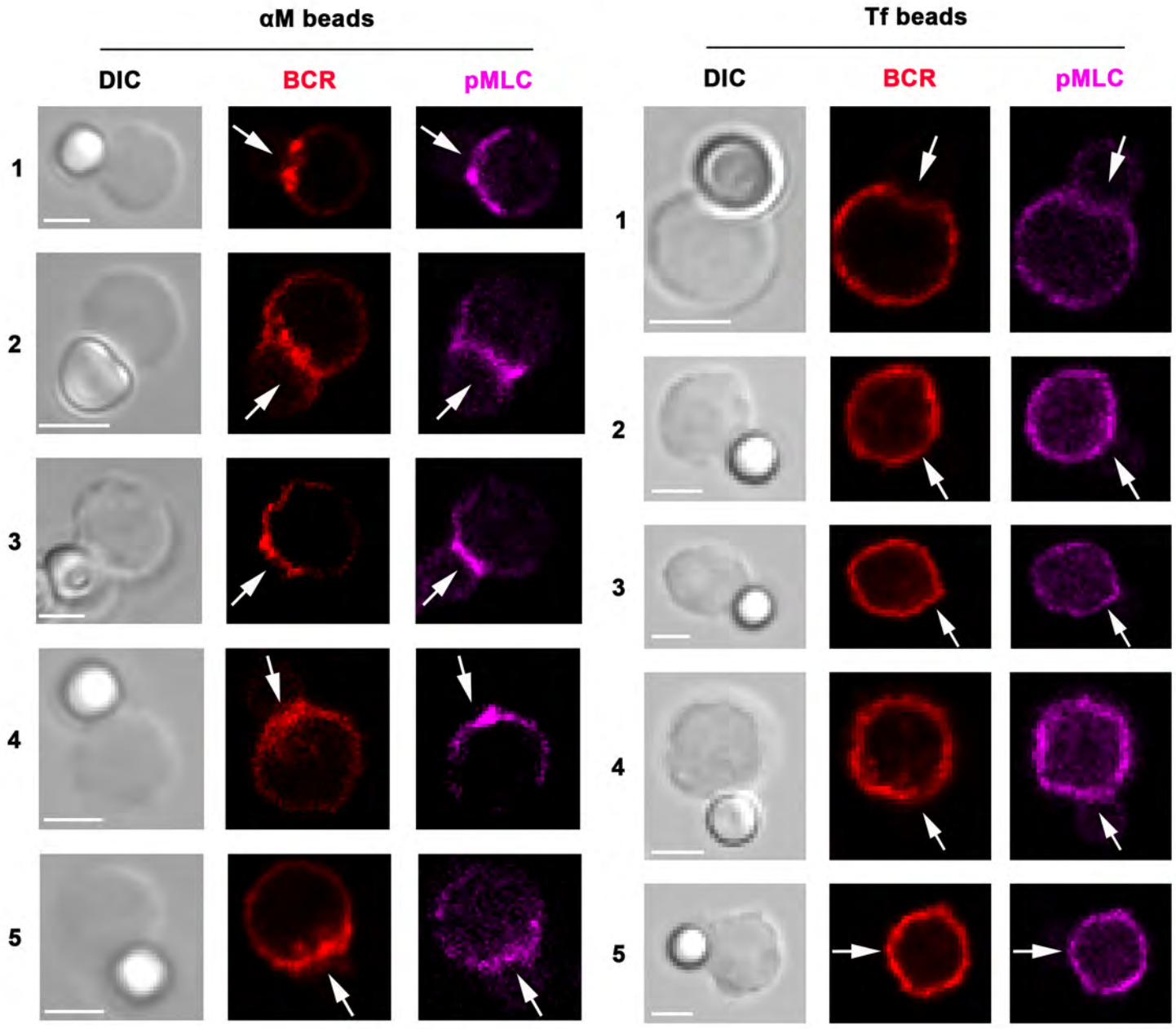

Figure 5- figure supplement 1

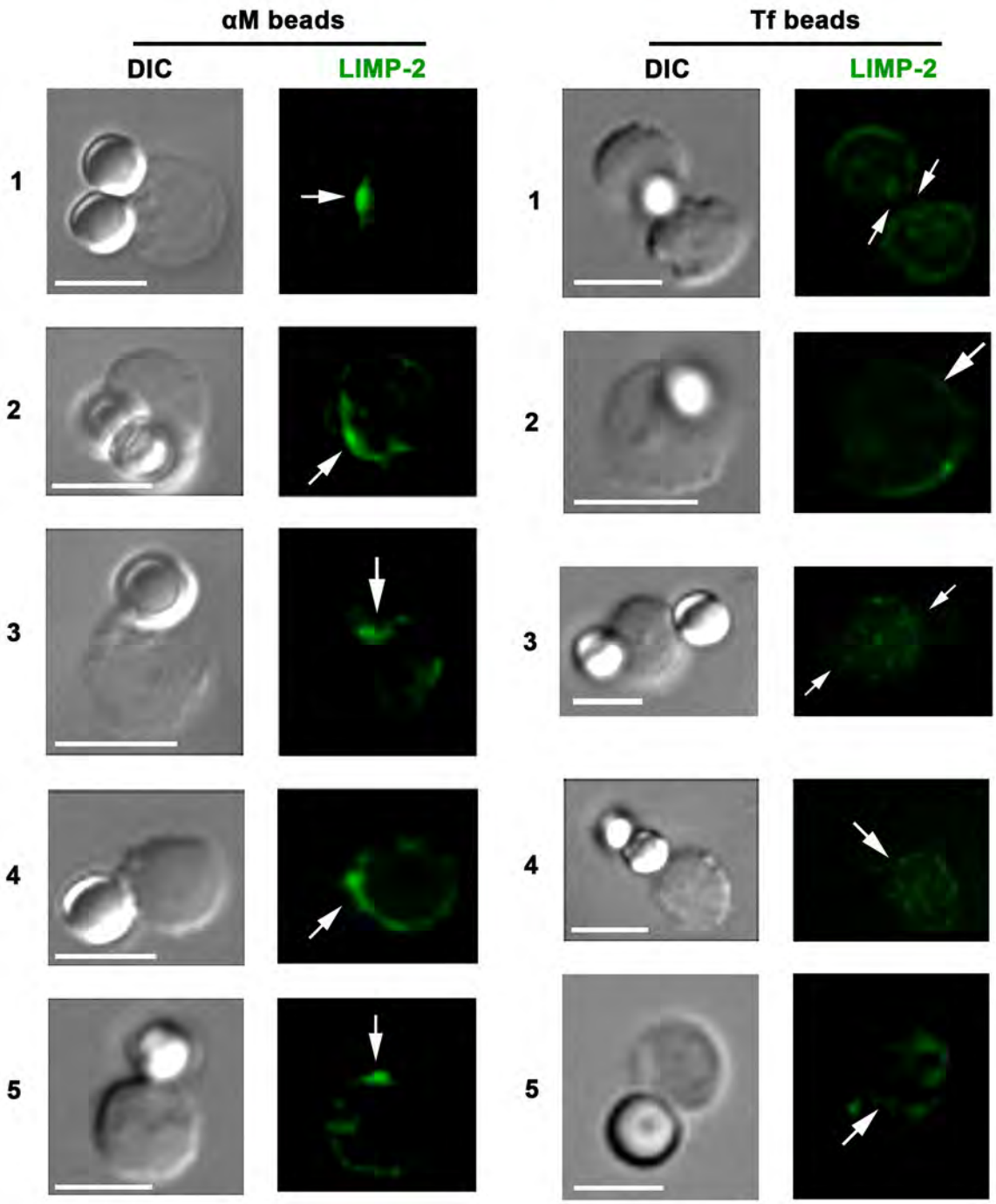

Figure 5- figure supplement 2

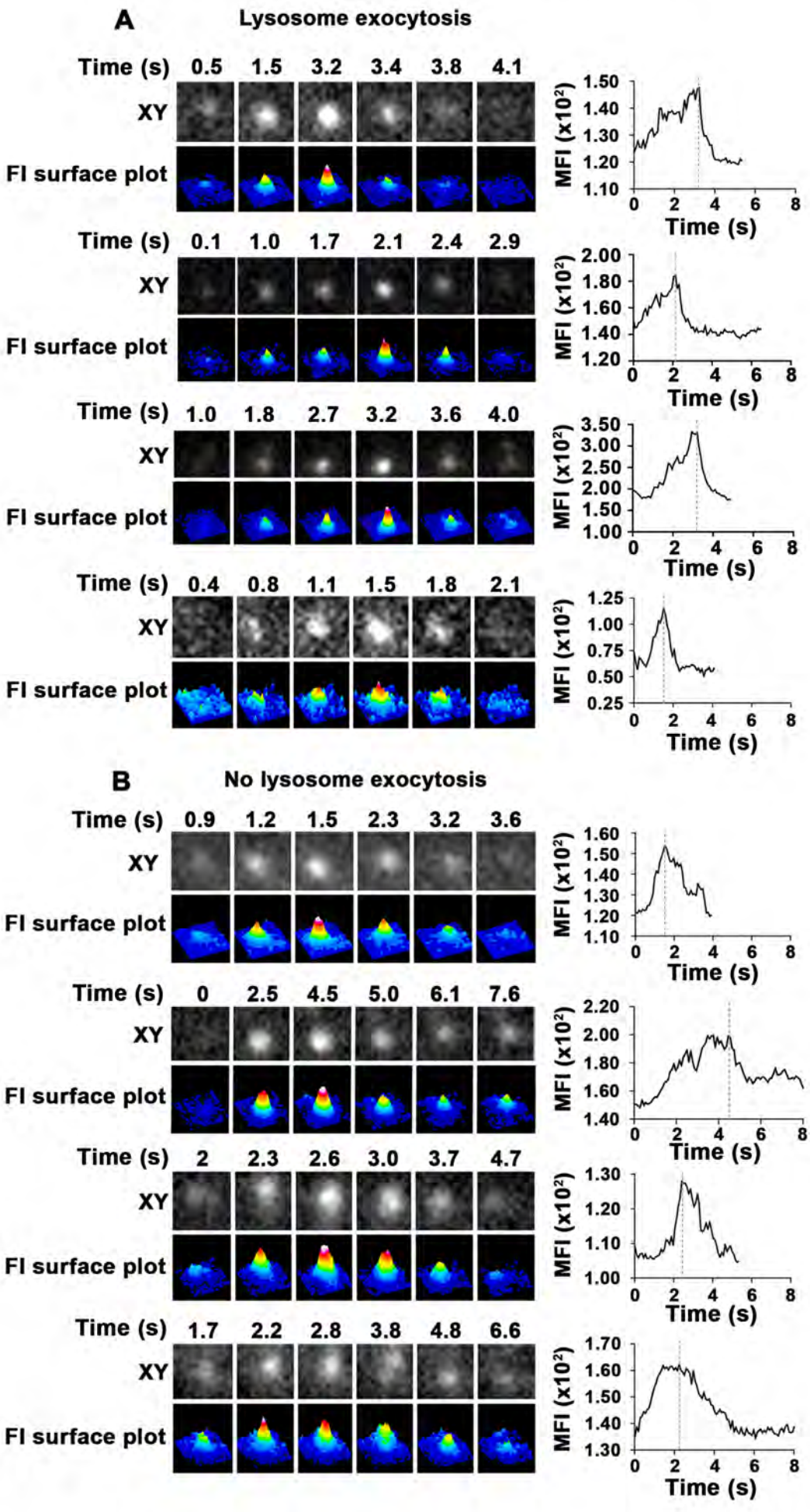

Figure 6- figure supplement 1

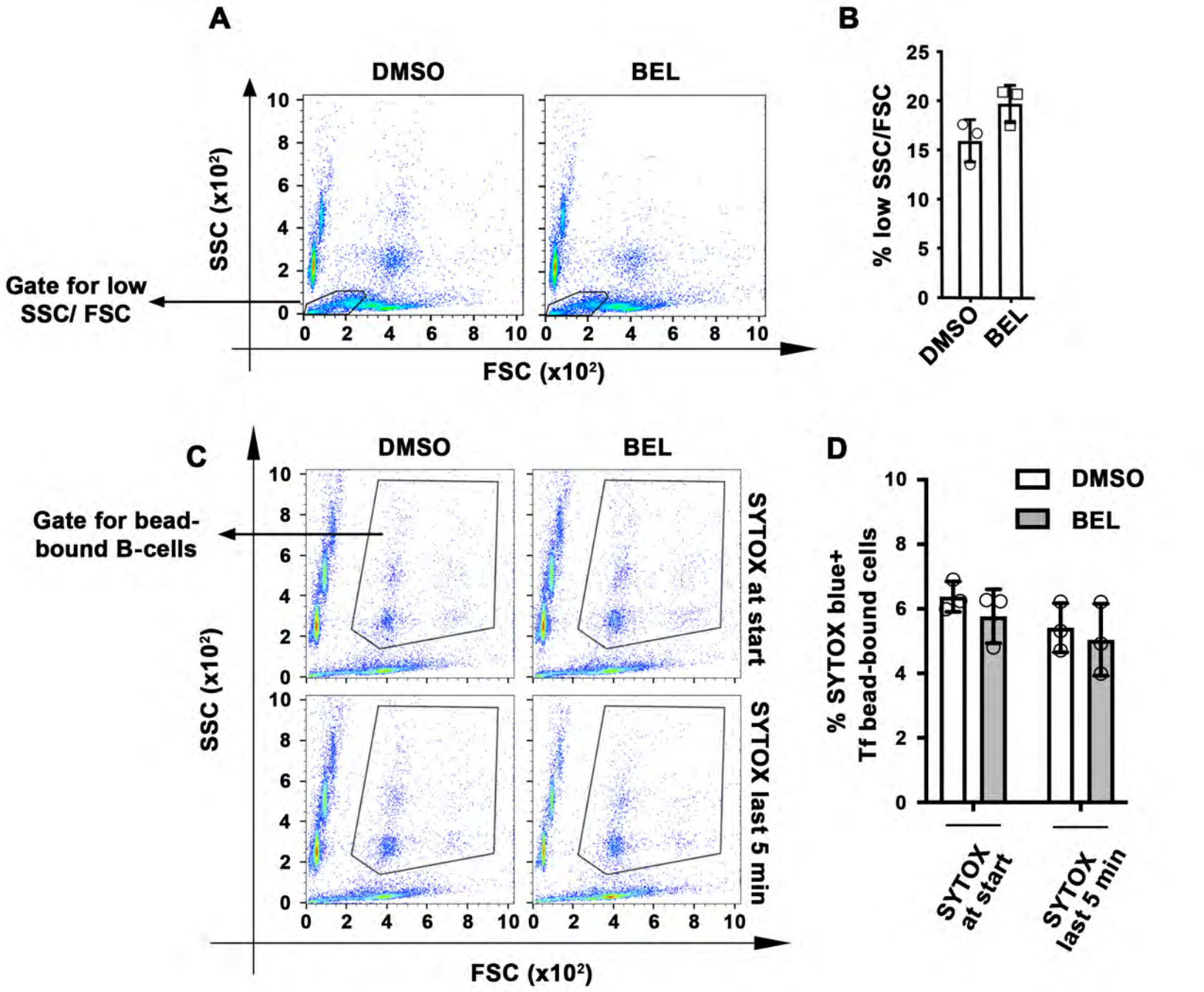

Figure 6- figure supplement 2